JGR Space Physics

RESEARCH ARTICLE
10.1029/2021JA029760

A Theoretical Framework of Chorus Wave Excitation

F. Zonca[1,2], X. Tao[3,4], and L. Chen[1,2,5]

[1]Center for Nonlinear Plasma Science and C.R. ENEA Frascati, Frascati, Italy, [2]Institute of Fusion Theory and Simulation and Department of Physics, Zhejiang University, Hangzhou, China, [3]CAS Key Laboratory of Geospace Environment, Department of Geophysics and Planetary Sciences, University of Science and Technology of China, Hefei, China, [4]CAS Center for Excellence in Comparative Planetology, Hefei, China, [5]Department of Physics and Astronomy, University of California, Irvine, CA, USA

Key Points:

- We derive a novel theoretical framework of chorus wave excitation based on classical field theoretical approach
- The chorus chirping rate originally proposed by Vomvoridis et al. (1982) is derived analytically for the first time
- We emphasize the analogy of chorus chirping with similar phenomena in fusion plasmas and free electron laser physics

Correspondence to:

F. Zonca,
fulvio.zonca@enea.it

Citation:

Zonca, F., Tao, X., & Chen, L. (2022). A theoretical framework of chorus wave excitation. *Journal of Geophysical Research: Space Physics*, *127*, e2021JA029760. https://doi.org/10.1029/2021JA029760

Received 6 JUL 2021
Accepted 11 JAN 2022

Author Contributions:

Conceptualization: F. Zonca, X. Tao, L. Chen
Methodology: F. Zonca, X. Tao, L. Chen
Software: F. Zonca, X. Tao, L. Chen

Abstract We propose a self-consistent theoretical framework of chorus wave excitation, which describes the evolution of the whistler fluctuation spectrum as well as the suprathermal electron distribution function. The renormalized hot electron response is cast in the form of a Dyson-like equation, which then leads to evolution equations for nonlinear fluctuation growth and frequency shift. This approach allows us to analytically derive for the first time exactly the same expression for the chorus chirping rate originally proposed by Vomvoridis et al. (1982). Chorus chirping is shown to correspond to maximization of wave particle power exchange, where each individual wave belonging to the whistler wave packet is characterized by small nonlinear frequency shift. We also show that different interpretations of chorus chirping proposed in published literature have a consistent reconciliation within the present theoretical framework, which further illuminates the analogy with similar phenomena in fusion plasmas and free electron laser physics.

1. Introduction

Chorus waves are whistler mode waves with frequency (ω) typically between one-tenth of and the electron cyclotron frequency (Ω) (see, e.g., Burtis & Helliwell, 1976; Tsurutani & Smith, 1974). These waves have been demonstrated to play important roles in energetic electron dynamics in the terrestrial magnetosphere. Chorus waves are responsible for the acceleration of a few hundred keV electrons to the MeV energy range, leading to the enhancement of MeV electron fluxes in the outer radiation belt during geomagnetically disturbed times (Bortnik & Thorne, 2007; Chen et al., 2007; Horne & Thorne, 1998; Horne et al., 2005; Reeves et al., 2013; Thorne et al., 2013). Furthermore, scattering of a few hundred eV to a few keV electrons by chorus waves into the atmosphere has been shown to be the dominant process in the formation of energetic electron pancake distributions (Tao et al., 2011), diffuse aurora (Thorne et al., 2010), and pulsating aurora (Miyoshi et al., 2010; Nishimura et al., 2010).

Chorus waves consist of quasi-coherent discrete elements with frequency chirping. In the terrestrial magnetosphere, the frequency of a chorus element may vary by a few hundred Hz to a few kHz in less than a second. Previous studies have established that coherent nonlinear wave-particle interactions play a key role in the frequency chirping, and have demonstrated that the chirping rate for rising tone chorus is proportional to the wave amplitude. Using a series of simulations, Vomvoridis et al. (1982) argued that, to maximize wave power transfer, the frequency chirping rate and the wave amplitude for parallel propagating chorus waves is related by

$$\frac{\partial\omega}{\partial t} = R\left(1 - \frac{v_r}{v_g}\right)^{-2}\omega_{tr}^2, \tag{1}$$

with $R = 1/2$. Here, v_r is the cyclotron resonant velocity, v_g is the wave group velocity, and $\omega_{tr}^2 = kv_\perp e\delta B/(mc)$ with $v_\perp$ the perpendicular velocity, k the wave number, and δB the wave amplitude. Theoretical interpretation of Equation 1 was proposed by Trakhtengerts et al. (2004) and Demekhov (2011), based on the assumption that a chorus element is formed as a succession of sidebands separated from each other by the trapping frequency ω_{tr} over time scales $2\pi/\omega_{tr}$. Meanwhile, for optimum cyclotron power exchange of electrons with a whistler wave in an inhomogeneous magnetic field, the growth rate is determined by a Backward Wave Oscillator (BWO) condition. Good agreement from comparisons of these chorus sweeping rate predictions with observations was reported by Trakhtengerts et al. (2004), Macúšová et al. (2010), and Tao et al. (2012). Another interpretation of Equation 1 was proposed by Omura et al. (2008), by assuming a constant value for the phase space density of phase-trapped electrons, and demonstrating that the resonant current density in the direction of wave electric field maximizes at $R = 0.4$, consistent with Equation 1 of Vomvoridis et al. (1982). Equation 1 has been verified by several different particle-in-cell (PIC) type simulations (Hikishima & Omura, 2012; Katoh & Omura, 2011, 2013; Tao et al., 2017a, 2017b) and an observational study (Cully et al., 2011). More recently, Mourenas et al. (2015) suggested using the nonlinear chorus growth rate from Shklyar and Matsumoto (2011), based on contributions from both trapped and untrapped resonant particles, to derive an analytical estimate of the value of $R = S^*$ maximizing this nonlinear growth rate. They obtained $R = S^* = 3/5$ in the case of oblique chorus waves.

Despite of Equation 1 being a huge success, its derivation was based either on simulations (Vomvoridis et al., 1982) or by assuming either a given behavior of the fluctuation spectrum (Demekhov, 2011; Trakhtengerts et al., 2004), or a specific form of the distribution function for phase trapped (Omura et al., 2008) and/or untrapped (Mourenas et al., 2015; Shklyar & Matsumoto, 2011) particles. Besides, Equation 1 was derived assuming the pre-existence of frequency chirping (Vomvoridis et al., 1982). The reason for frequency chirping of chorus was explained by Omura and Nunn (2011) due to the nonlinear current parallel to the wave magnetic field (J_B), which causes frequency shift. In this paper, we propose a new first principle based theoretical framework for chorus wave excitation that addresses the dynamic evolution of the fluctuation spectrum and its interaction with trapped as well as untrapped resonant particles on the same footing. This *self-consistent* analysis is a novelty of the present approach with respect to previous studies. By keeping the dominant long-term nonlinear response in the distribution function, we obtain an equation for the evolution of the distribution function of hot electrons in the form of a Dyson-like equation (Dyson, 1949; Schwinger, 1951). This model (Chen & Zonca, 2016; Zonca et al., 2015b) explains chirping as a result of the dynamic nonlinear spectrum evolution due to coherent excitation of a narrow fluctuation spectrum that is shifting in time out of a broad and dense whistler wave spectrum. Furthermore, it demonstrates the ballistic propagation of resonant structures in the hot electron phase space (Chen & Zonca, 2016; Zonca et al., 2015b), and analytically shows that maximization of wave power transfer leads to $R = 1/2$ and Equation 1, fully coincident with previous results of Vomvoridis et al. (1982). At last, the present theoretical framework illuminates why the original approach by Omura and Nunn (2011), based on the nonlinear frequency shift due to J_B, yields the correct estimate of chorus chirping rate starting from a different perspective.

In the present analysis, we focus on the nonlinear dynamics of phase-space structures of correlated electrons, which are due to nonlinear wave-particle interactions that predominantly occur "in the downstream of equator," after the whistler wave packets have traveled through the suprathermal electron source region localized near the equator itself. In this respect, we construct the theoretical framework that underlies the numerical simulation analysis of Tao et al. (2017a), where we showed that the time scale of chorus nonlinear dynamics is $\sim\mathcal{O}(2\pi/\omega_{tr})$ characteristic of nonperturbative wave-particle interactions (Chen & Zonca, 2016; Zonca et al., 2015b), and that the wave growth is mainly due to phase bunched electrons. This work is a more in-depth analysis based on earlier preliminary theoretical approach (Zonca et al., 2017). The present analysis can also be considered as theoretical building block for a recent simulation work (Tao et al., 2021), which proposes a novel phenomenological interpretation for chorus, called the "Trap-Release-Amplify" (TaRA) model. The TaRA model establishes a connection between the upstream and downstream of equator regions in chorus dynamics, and shows that phase-locked electrons in the upstream region selectively amplify wave packets with a chirping rate that is fully consistent with the Helliwell analysis for a nonuniform background magnetic field (Helliwell, 1967). Meanwhile, in the downstream region, the nonlinear wave-particle analysis in the TaRA model yields the chorus chirping expression of Equation 1, consistent with Vomvoridis et al. (1982) as well as with former (Tao et al., 2017a; Zonca et al., 2017) and present analyses.

The structure of the paper is as follows. Section 2 discusses the present novel theoretical framework based on the self-consistent solution of wave equations (Section 2.1) and of nonlinear phase-space dynamics (Section 2.2). Reduced model equations for the nonlinear evolution of spectral intensity and phase shift are presented in Section 3. These are then applied to the investigation of chorus excitation and nonlinear dynamics in Section 4. Finally, Section 5 is devoted to discussion and concluding remarks. Four appendixes are further devoted to detailed derivations for interested readers.

2. Theory

Let us adopt the standard hybrid approach, where the Earth's magnetosphere plasma is assumed to consist of a neutralizing cold thermal ion background and a "core" (c) and "hot" (h) electron components. From Ampère's law, and separating the current density perturbation $\delta\boldsymbol{J}$ in "core" (c) and "hot" (h) components, for parallel propagating transverse electromagnetic waves we have

$$\left(1-\frac{k^2c^2}{\omega^2}\right)\delta\boldsymbol{E}_\perp+\frac{4\pi i}{\omega}\delta\boldsymbol{J}_c\equiv\boldsymbol{\epsilon}_\perp\cdot\delta\boldsymbol{E}_\perp-\frac{k^2c^2}{\omega^2}\delta\boldsymbol{E}_\perp=-\frac{4\pi i}{\omega}\delta\boldsymbol{J}_h, \tag{2}$$

where considering "core" electrons as a cold fluid with density n, $\boldsymbol{\epsilon}_\perp$ is the usual cold plasma dielectric tensor

$$\boldsymbol{\epsilon}_\perp\cdot\delta\boldsymbol{E}_\perp=\left(1+\frac{\omega_p^2}{\Omega^2-\omega^2}\right)\delta\boldsymbol{E}_\perp-i\frac{\Omega}{\omega}\frac{\omega_p^2}{\Omega^2-\omega^2}\hat{\boldsymbol{z}}\times\delta\boldsymbol{E}_\perp, \tag{3}$$

with $\hat{\boldsymbol{z}}$ the unit vector along the Earth's magnetic field and, adopting standard notation, $\omega_p^2=4\pi ne^2/m$ is the electron plasma frequency, and $\Omega=eB/(mc)$ is the electron cyclotron frequency, with e the positive electron charge and m the electron mass.

For a typical rising tone chorus event that we are addressing here, the characteristic nonlinear time and duration are much shorter than the time it takes for a whistler wave to propagate from the equator to either southern or northern ionospheres. Thus, we assume a wave packet description for chorus, which has a dense (nearly continuous) spectrum and is nearly degenerate with a parallel propagating whistler wave with right circular polarization; i.e., $\boldsymbol{k}=\hat{\boldsymbol{z}}k$, $\delta E_z=\delta B_z=0$, $\delta E_y=i\delta E_x$, and $\delta B_y=i\delta B_x$, with $\delta B_y=(ck/\omega)\delta E_x$. This yields

$$\boldsymbol{\epsilon}_\perp\cdot\delta\boldsymbol{E}_\perp\simeq\left(1+\frac{\omega_p^2}{\omega(\Omega-\omega)}\right)\delta\boldsymbol{E}_\perp. \tag{4}$$

Thus, the problem of transverse chorus wave packet interacting with hot electrons can be approximately cast as (Nunn, 1974; Omura & Matsumoto, 1982; Omura & Nunn, 2011; Omura et al., 2008)

$$\left(1+\frac{\omega_p^2}{\omega(\Omega-\omega)}\right)\delta\boldsymbol{E}_\perp-\frac{k^2c^2}{\omega^2}\delta\boldsymbol{E}_\perp=-\frac{4\pi i}{\omega}\delta\boldsymbol{J}_h, \tag{5}$$

where the right-hand side can be formally treated as a perturbation to the lowest order propagation of the whistler wave packet due to the low density of hot electrons.

2.1. Wave Equations

Let us introduce the whistler wave dielectric constant, ϵ_w, and dispersion function, D_w, such as

$$\epsilon_w=1+\frac{\omega_p^2}{\omega(\Omega-\omega)},\quad D_w=\epsilon_w-\frac{k^2c^2}{\omega^2}. \tag{6}$$

The elements of the whistler wave packet can be written as

$$\delta\boldsymbol{E}_\perp(z,t)=\frac{1}{2}\sum_k\left(e^{iS_k(z,t)}\delta\bar{\boldsymbol{E}}_{\perp k}(z,t)+c.c.\right), \tag{7}$$

with $c.c.$ denoting the complex conjugate, denoted in the following with a * superscript, and the eikonal S_k is defined such that $\omega_k=-\partial_tS_k$, $k=\partial_zS_k$, which satisfy the WKB dispersion relation

$$D_w(z,k(z),\omega_k)=0. \tag{8}$$

Meanwhile, letting

$$\delta\bar{\boldsymbol{E}}_{\perp k}(z,t)=\hat{\boldsymbol{e}}|\delta\bar{\boldsymbol{E}}_{\perp k}(z,t)|e^{i\varphi_k(z,t)}, \tag{9}$$

with $\hat{\boldsymbol{e}}$ the polarization vector defined such $\hat{\boldsymbol{e}}\cdot\hat{\boldsymbol{z}}=0$ and $\hat{\boldsymbol{e}}\cdot\hat{\boldsymbol{e}}^*=1$; and introducing wave intensity or action as

$$I_k(z,t) \equiv |\partial D_w/\partial k|\, |\delta \bar{\boldsymbol{E}}_{\perp k}(z,t)|^2, \tag{10}$$

the evolution equation for $I_k(z, t)$ is (Bernstein & Baldwin, 1977; McDonald, 1988)

$$\left(\frac{\partial}{\partial t} + v_{gk}\frac{\partial}{\partial z}\right) I_k(z,t) = 2\gamma_k I_k(z,t), \tag{11}$$

where $v_{gk} = -(\partial D_w/\partial \omega_k)^{-1}\partial D_w/\partial k$ is the wave packet group velocity and

$$\gamma_k = -\frac{D^1_{Ak}}{\partial D_w/\partial \omega_k} \tag{12}$$

represents the wave packet driving rate due to the hot electrons. In fact, noting $\partial_z \partial_k D_w = 0$ (McDonald, 1988),

$$D^1_{Ak} = \mathbb{I}\mathrm{m}\left(\frac{4\pi i}{\omega_k}\frac{\delta \bar{\boldsymbol{J}}_{hk}\cdot \delta \bar{\boldsymbol{E}}^*_{\perp k}}{|\delta \bar{\boldsymbol{E}}_{\perp k}(z,t)|^2}\right). \tag{13}$$

Meanwhile, the phase shift $\varphi_k(z, t)$ is given by (Bernstein & Baldwin, 1977; McDonald, 1988)

$$\left(\frac{\partial}{\partial t} + v_{gk}\frac{\partial}{\partial z}\right) \varphi_k(z,t) = \frac{D^1_{Rk}}{\partial D_w/\partial \omega_k}, \tag{14}$$

where

$$D^1_{Rk} = \mathbb{R}\mathrm{e}\left(\frac{4\pi i}{\omega_k}\frac{\delta \bar{\boldsymbol{J}}_{hk}\cdot \delta \bar{\boldsymbol{E}}^*_{\perp k}}{|\delta \bar{\boldsymbol{E}}_{\perp k}(z,t)|^2}\right). \tag{15}$$

Thus, all relevant nonlinear physics is included in the wave-particle interaction and the two functions $W(z, t, \omega)$ and $\Gamma(z, t, \omega)$, representing, respectively, the phase shift and driving rate due to hot electrons

$$W(z,t,\omega) + i\Gamma(z,t,\omega) \equiv -\left.\frac{4\pi i}{\omega \partial D_w/\partial \omega}\frac{\delta \bar{\boldsymbol{J}}_{hk}\cdot \delta \bar{\boldsymbol{E}}^*_{\perp k}}{|\delta \bar{\boldsymbol{E}}_{\perp k}(z,t)|^2}\right|_{k=K(z,\omega)}, \tag{16}$$

where $k = K(z, \omega)$ is obtained from the solution of the linear dispersion relation, $D_w = 0$. Noting that, in the complex wave representation adopted here, $\delta \bar{\boldsymbol{J}}_{hk}\cdot \delta \bar{\boldsymbol{E}}^*_{\perp k} = -i(\omega/kc)\delta \bar{\boldsymbol{J}}_{hk}\cdot \delta \bar{\boldsymbol{B}}^*_{\perp k}$ for the considered right circularly polarized parallel propagating whistler wave packet, Equations 10–16 coincide with those adopted by Nunn (1974) and Omura and Nunn (2011). With the definition of $W(z, t, \omega)$ and $\Gamma(z, t, \omega)$ as in Equation 16, the right-hand side of Equations 11 and 14 become, respectively, $2\Gamma(z, t, \omega)I(z, t, \omega)$ and $-W(z, t, \omega)$, where $I(z, t, \omega) \equiv I_k(z, t)|_{k=K(z,\omega)}$ and the group velocity on the left-hand side has to be interpreted as $v_{g\omega}(z) = v_{gk}(z)|_{k=K(z,\omega)}$.

Equation 16 can be rewritten expressing the wave particle power transfer in terms of the hot electron response. In fact, noting the hot electron right-hand cyclotron motion in the ambient magnetic field

$$\boldsymbol{v}\cdot \delta \bar{\boldsymbol{E}}^*_{\perp k} = -i v_\perp e^{-i\alpha}\delta \bar{E}^*_k, \tag{17}$$

where $v_\perp$ (and $v_\parallel$) indicate the perpendicular (and parallel, respectively) velocity with respect to the ambient Earth's magnetic field, α is the gyrophase ($\dot{\alpha} = \Omega$); and we have denoted $\delta \bar{E}_k \equiv \left(\delta \bar{\boldsymbol{E}}_{\perp k}\right)_x$ for brevity. Meanwhile, hot electron response can be represented as

$$f(\boldsymbol{v},z,t) = f_0(\boldsymbol{v},z,t) + \frac{1}{2}\sum_k \left(e^{iS_k(z,t)+i\alpha}\delta \bar{f}_k(\boldsymbol{v},z,t) + c.c.\right), \tag{18}$$

while the hot electron perpendicular current is given by

$$\delta \boldsymbol{J}_h(z,t) = \frac{1}{2}\sum_k \left(e^{iS_k(z,t)}\delta \bar{\boldsymbol{J}}_{hk}(z,t) + c.c.\right). \tag{19}$$

Thus, combining Equations 17–19, we have

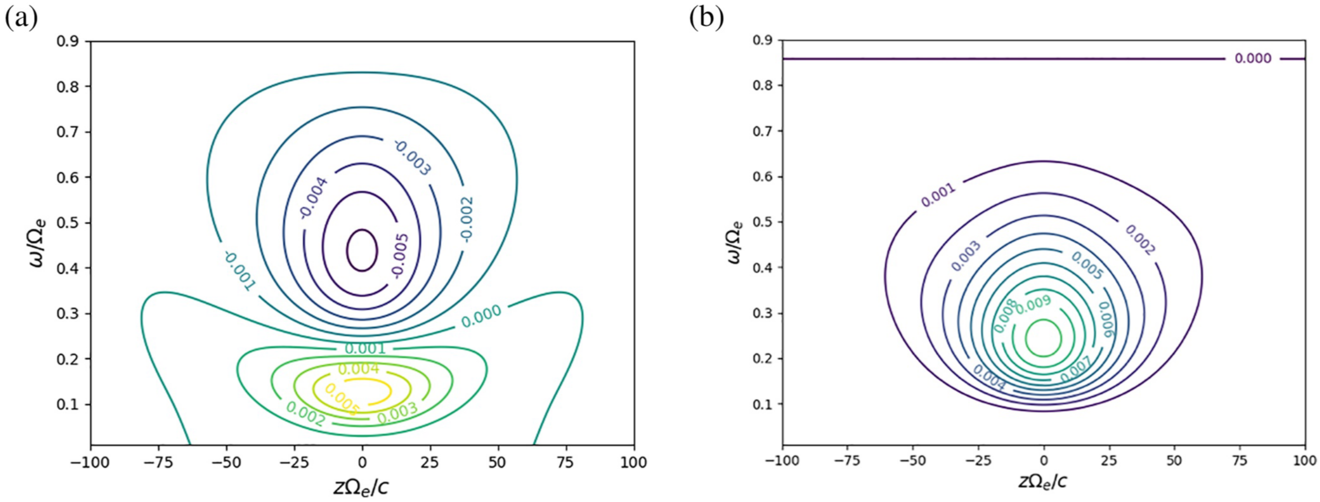

Figure 1. Contour plots of $W(z, t = 0, \omega)/\Omega_e$ (a) and $\Gamma(z, t = 0, \omega)/\Omega_e$ (b) are shown for normalized parameters $\omega_p/\Omega_e = 5$, $n_e/n = 6 \times 10^{-3}$, $w_{\parallel e} = 0.2c$, $w_{\perp e} = 0.53c$, $\xi = 8.62 \times 10^{-5}\Omega_e^2/c^2$.

$$-\frac{4\pi i}{\omega}\frac{\delta\bar{\boldsymbol{J}}_{hk}\cdot\delta\bar{\boldsymbol{E}}^*_{\perp k}}{|\delta\bar{\boldsymbol{E}}_{\perp k}(z,t)|^2}\bigg|_{k=K(z,\omega)} = \left\langle \frac{4\pi e}{\omega}\frac{\boldsymbol{v}_\perp}{2}\frac{\delta\bar{E}^*_k\delta\bar{f}_k}{|\delta\bar{E}_k|^2}\right\rangle = \frac{\omega_p^2}{n\omega}\left\langle \frac{\boldsymbol{v}_\perp^2/2}{\Omega + k\boldsymbol{v}_\parallel - \omega}\left[\frac{k}{\omega}\frac{\partial f_0}{\partial \boldsymbol{v}_\parallel} + \left(1 - \frac{k\boldsymbol{v}_\parallel}{\omega}\right)\frac{1}{v_\perp}\frac{\partial f_0}{\partial \boldsymbol{v}_\perp}\right]\right\rangle. \tag{20}$$

Here, we have noted that $|\delta\bar{\boldsymbol{E}}_{\perp k}(z,t)|^2 = 2|\delta\bar{E}_k|^2$, angular brackets $\langle\dots\rangle$ denote velocity space integration, and assumed Equation 31 for expressing $\delta\bar{f}_k$, which will be derived in Section 2.2. Furthermore, it is important to emphasize that f_0 is the $k = 0$ component of the hot electron distribution function, which evolves in time due to the nonlinear wave-particle interactions. Thus, f_0 is the "equilibrium" distribution function assumed initially only at $t = 0$.

Since the source region of chorus is localized near the equator, we follow the usual practice of assuming a model of Earth's dipole magnetic field in the form $B = B_e(1 + \xi z^2)$ (Helliwell, 1967), with B_e representing the magnetic field strength at the equator and $\xi^{-1/2}$ the nonuniformity scale length. Thus, we take a model $\Omega = \Omega_e(1 + \xi z^2)$ with Ω_e the (nonrelativistic) electron cyclotron frequency at the equator. Meanwhile, following Tao (2014), we assume an "initial" hot electron f_0 in the form of a bi-Maxwellian

$$f_0|_{t=0} = \frac{n_0}{(2\pi)^{3/2}w_\parallel w_\perp^2}\exp\left(-v_\perp^2/(2w_\perp^2) - v_\parallel^2/(2w_\parallel^2)\right), \tag{21}$$

where $n_0 = \zeta^2 n_e$, $w_\parallel = w_{\parallel e}$, $w_\perp = \zeta w_{\perp e}$, and $\zeta^{-2} = 1 + A\xi z^2/(1 + \xi z^2)$, with $A \equiv w_{\perp e}^2/w_{\parallel e}^2 - 1 > 0$ the anisotropy index computed at the equator (cf. Appendix A). Contour plots of the "initial" (linear) functions $W(z, t = 0, \omega)$ and $\Gamma(z, t = 0, \omega)$ are given in Figure 1, for normalized parameters $\omega_p/\Omega_e = 5$, $n_e/n = 6 \times 10^{-3}$, $w_{\parallel e} = 0.2c$, $w_{\perp e} = 0.53c$, $\xi = 8.62 \times 10^{-5}\Omega_e^2/c^2$ (Tao, 2014). From Equations 16 and 20, it can be shown that both $W(z, t, \omega)$ and $\Gamma(z, t, \omega)$ scale as $\sim\zeta^4$, which accounts for most of the spatial nonuniformity of hot electron response, characterized by the length scale $(A\xi)^{-1/2}$ as clearly illustrated by Figure 1 (cf. Appendix A). Thus, at the leading order, hot electrons can be considered as a nonuniform source neglecting magnetic field nonuniformity. Although not necessary, this assumption will help simplifying our analytical derivations in the remainder of this work, starting with Section 2.2 (cf. Appendix A for more details).

With the knowledge of $W(z, t, \omega)$ and $\Gamma(z, t, \omega)$, the nonlinear evolution of the chorus spectrum can be derived from the integration of Equations 11 and 14 along the characteristics, recalling that the right-hand sides are, respectively, $2\Gamma(z, t, \omega)I(z, t, \omega)$ and $-W(z, t, \omega)$ as noted above. Thus, solutions are formally written as

$$I(z,t,\omega) = I_{\omega 0}\left(T_\omega^{-1}(T_\omega(z) - t)\right)\exp\left(2\int_{T_\omega^{-1}(T_\omega(z)-t)}^{z}\frac{dz'}{v_{g\omega}(z')}\Gamma(z', t - T_\omega(z) + T_\omega(z'), \omega)\right), \tag{22}$$

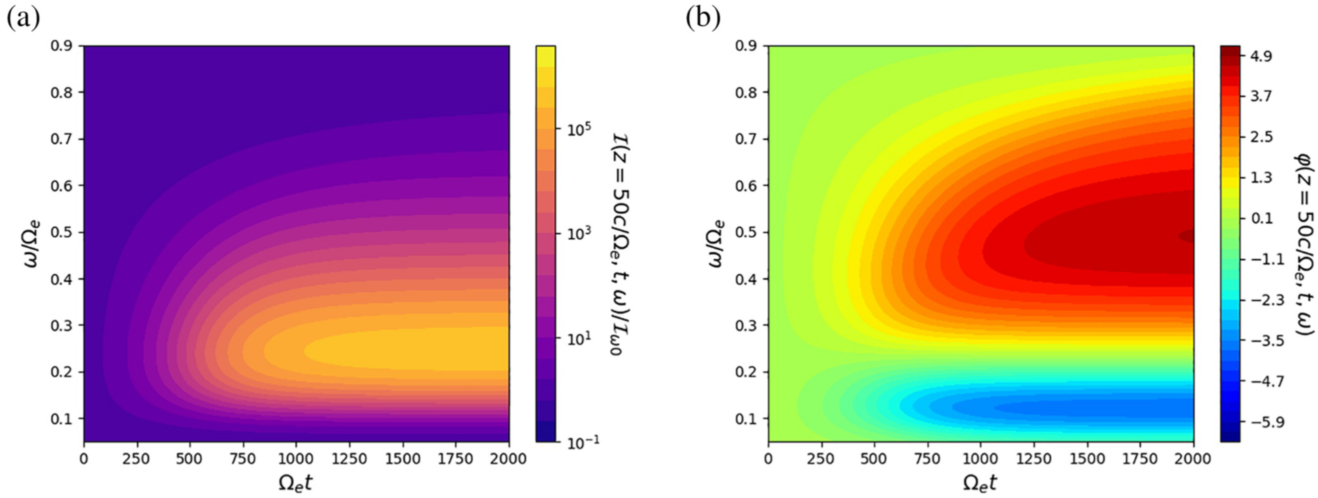

Figure 2. Contour plots of $I(z, t, \omega)/I_{\omega 0}$ (a) and $\varphi(z, t, \omega)$ (b) are shown for the linear evolution of the whistler wave packet and the same normalized parameters of Figure 1. Here, $I_{\omega 0}$ = const and $\varphi_{\omega 0} = 0$ have been assumed together with $z\Omega_e/c = 50$.

for the wave packet intensity $I(z, t, \omega)$, where

$$T_\omega(z) \equiv \int_0^z \frac{dz'}{v_{g\omega}(z')}. \tag{23}$$

Meanwhile, a similar solution can be written for phase shift $\varphi(z, t, \omega) \equiv \varphi_k(z, t)|_{k=K(z,\omega)}$

$$\varphi(z,t,\omega) = \varphi_{\omega 0}\left(T_\omega^{-1}(T_\omega(z)-t)\right) - \int_{T_\omega^{-1}(T_\omega(z)-t)}^{z} \frac{dz'}{v_{g\omega}(z')} W(z', t - T_\omega(z) + T_\omega(z'), \omega). \tag{24}$$

In the linear limit, where $W(z, t, \omega) = W(z, t = 0, \omega)$ and $\Gamma(z, t, \omega) = \Gamma(z, t = 0, \omega)$, Equations 22 and 24 are readily computed and corresponding solutions are shown in the contour plots of Figure 2 for the same parameters of Figure 1 and $z\Omega_e/c = 50$. Nonlinear evolution is all embedded in the time dependence of $W(z, t, \omega)$ and $\Gamma(z, t, \omega)$. In particular, we will show below that chorus chirping may be understood as the spectral frequency peak of $I(z, t, \omega)$ at a given spatial position shifting in time. Meanwhile, since the growth of the spectral peak is due to spontaneous emission of whistler waves excited by hot electrons at the proper (instantaneous) wavelength and frequency, chorus nonlinear evolution is, thus, clearly associated with maximization of wave particle power transfer (Omura et al., 2008; Trakhtengerts et al., 2004; Vomvoridis et al., 1982), as noted to be the case also for Alfvénic fluctuations in magnetized fusion plasmas (Chen & Zonca, 2016; Zonca et al., 2015b). We will later come back to this very important point, with more insights and comments on the underlying physics. Summarizing, this analysis shows that chorus chirping rate can be predicted via analyzing $\partial_t\Gamma(z, t, \omega)$. In particular, $\partial_t\Gamma$ can be derived from $\partial_t f_0$, that is from manipulation of the Dyson-like equation, given in Section 2.2, as remarked in Section 1. This derivation is carried out in Section 3, where we also show how $\partial_t\Gamma(z, t, \omega)$ and $\partial_t W(z, t, \omega)$ are interlinked (Zonca et al., 2017).

2.2. Phase-Space Dynamics

As shown in Section 2.1, hot electrons are localized about the equator and plasma nonuniformity effects are dominated by the $\sim\zeta^4$ scaling of both $W(z, t, \omega)$ and $\Gamma(z, t, \omega)$. Thus, as noted in Appendix A, hot electrons can be approximated as a nonuniform source, characterized by the length scale $(A\xi)^{-1/2}$, neglecting magnetic field nonuniformity. This assumption helps simplifying our analytical derivations below and, thus, we choose to adopt it in the following. In order to simplify presentation, we also assume $\omega^2/\omega_p^2 \ll 1$, so that expressions of $W(z, t, \omega)$ and $\Gamma(z, t, \omega)$ are reduced to

$$W(z,t,\omega) + i\Gamma(z,t,\omega) = \frac{n_e}{n}\zeta^4 \frac{\omega(\Omega_e-\omega)^2}{\Omega_e} \left\langle \frac{1}{\Omega_e + kv_\parallel - \omega} \left[\frac{kv_\perp^2}{2\omega}\frac{\partial}{\partial v_\parallel} - \frac{\Omega_e}{\omega} \right] \hat{f}_0 \right\rangle, \tag{25}$$

Here and in the following, $k = K(z = 0, \omega)$ will always be assumed as obtained from the solution of the linear dispersion relation, $D_w = 0$. Meanwhile, as illustrated in Appendix A, we have integrated Equation 20 by parts in $v_\perp$, extracted the expected hot electron nonuniformity scaling $\sim\zeta^4$, and denoted the response neglecting magnetic field nonuniformity as $f_0 \equiv n_e \hat{f}_0$. Equation 25 suggests the connection of the phase shift and driving rate by a localized hot electron source with that by a uniform hot electron source in uniform magnetic field. To make this more explicit, let us introduce the rescaled phase shift and driving rate, $\bar{W}(z,t,\omega)$ and $\bar{\Gamma}(z,t,\omega)$, defined as

$$W(z,t,\omega) + i\Gamma(z,t,\omega) \equiv \zeta^4 \frac{\omega(\Omega_e - \omega)^2}{\Omega_e^2} \left(1 - \frac{v_{r\omega}}{v_{g\omega}}\right)^{-2} \left[\bar{W}(z,t,\omega) + i\bar{\Gamma}(z,t,\omega)\right], \tag{26}$$

where $v_{r\omega} \equiv (\omega - \Omega_e)/k$ is the resonant velocity, and $v_{g\omega} = v_{g\omega}(z = 0)$ is the group velocity at the equator, defined below Equation 16. Thus, we rewrite Equation 25 as

$$\bar{W}(z,t,\omega) + i\bar{\Gamma}(z,t,\omega) = \frac{n_e}{n} \left(1 - \frac{v_{r\omega}}{v_{g\omega}}\right)^2 \left\langle \frac{\Omega_e}{\Omega_e + kv_\parallel - \omega} \left[\frac{kv_\perp^2}{2\omega}\frac{\partial}{\partial v_\parallel} - \frac{\Omega_e}{\omega}\right] \hat{f}_0 \right\rangle. \tag{27}$$

The usefulness of introducing the factor $(1 - v_{r\omega}/v_{g\omega})^2$, where both resonant and group velocity are computed at $z = 0$, will be clarified in Section 3. There, we will also show that residual spatiotemporal dependences of $\hat{f}_0$, $\bar{W}$ and $\bar{\Gamma}$ will be via $t - z/v_{g\omega}$.

In the presence of a fluctuation spectrum in the form of Equation 7, the hot electrons distribution function $f \equiv n_e \hat{f}$ can be written as

$$\hat{f}(z,t) = \hat{f}_0(z,t) + \frac{1}{2}\sum_k \left(e^{iS_k(z,t)+i\alpha}\delta\hat{\bar{f}}_k(z,t) + c.c.\right), \tag{28}$$

where $\hat{f}_0$, introduced in Equation 25, denotes the $k = 0$ component of $\hat{f}$; and, for brevity, we have omitted the velocity space dependences of hot electron response. Similar to Equation 18, Equation 28 follows from the fact that, given the chorus wave packet polarization properties discussed in Section 2.1

$$\frac{e}{m}\left(\delta\bar{\boldsymbol{E}}_k + \frac{\boldsymbol{v}\times\delta\bar{\boldsymbol{B}}_k}{c}\right)\cdot\frac{\partial}{\partial\boldsymbol{v}} = i\frac{e}{m}v_\perp\delta\bar{E}_k e^{i\alpha}\left[\frac{k}{\omega}\frac{\partial}{\partial v_\parallel} + \left(1 - \frac{kv_\parallel}{\omega}\right)\left(\frac{1}{v_\perp}\frac{\partial}{\partial v_\perp} + \frac{i}{v_\perp^2}\frac{\partial}{\partial\alpha}\right)\right]. \tag{29}$$

The evolution equation for $\hat{f}_0$ can be obtained from the Vlasov equation

$$\begin{aligned}(\partial_t + v_\parallel\partial_z)\,\hat{f}_0 \quad = \quad & \frac{1}{4}\sum_k i\frac{e}{m}v_\perp\delta\bar{E}_k\left[\frac{k}{\omega}\frac{\partial}{\partial v_\parallel} + \left(1 - \frac{kv_\parallel}{\omega}\right)\left(\frac{1}{v_\perp}\frac{\partial}{\partial v_\perp} + \frac{1}{v_\perp^2}\right)\right]\delta\hat{\bar{f}}_k^* \\ & -\frac{1}{4}\sum_k i\frac{e}{m}v_\perp\delta\bar{E}_k^*\left[\frac{k}{\omega}\frac{\partial}{\partial v_\parallel} + \left(1 - \frac{kv_\parallel}{\omega}\right)\left(\frac{1}{v_\perp}\frac{\partial}{\partial v_\perp} + \frac{1}{v_\perp^2}\right)\right]\delta\hat{\bar{f}}_k.\end{aligned} \tag{30}$$

Meanwhile, the fluctuating component of the hot electron response is given by

$$\begin{aligned}\mathcal{L}_k\delta\hat{\bar{f}}_k \quad \equiv \quad & \left[kv_\parallel + \Omega_e - \omega - i\left(\partial_t + v_\parallel\partial_z\right)\right]\delta\hat{\bar{f}}_k \\ = \; & \frac{e}{m}v_\perp\delta\bar{E}_k\left[\frac{k}{\omega}\frac{\partial}{\partial v_\parallel} + \left(1 - \frac{kv_\parallel}{\omega}\right)\frac{1}{v_\perp}\frac{\partial}{\partial v_\perp}\right]\hat{f}_0.\end{aligned} \tag{31}$$

Here, $\mathcal{L}_k$ is a first-order partial differential operator that can be "formally inverted" as propagator $\mathcal{L}_k^{-1}$, which is an integral operator. Equation 31 applies both linearly and nonlinearly; i.e., when $\hat{f}_0$ is evolving in time due to resonant wave-particle interactions. In particular, the action of the $(\partial_t + v_\parallel\partial_z)$ operator on the phase modulation due to $\delta\bar{E}_k = |\delta\bar{E}_k|e^{i\varphi_k}$ must be computed noting that the hot electron induced frequency (Δ_ω) and wave number (Δ_k) shifts due to an incremental change in the fluctuation spectrum still satisfy the whistler wave dispersion relation with good approximation. This assumption is based on observations that chorus waves propagate in whistler mode; and it is consistent with the interpretation of chorus chirping as "whistler seeds" that are excited in sequence and amplified by wave particle resonant interactions with hot electrons originally proposed by (Omura & Nunn, 2011). Thus, ω and k in Equations 30 and 31 denote the wave packet frequency and wave number in the presence of the hot electron source and the finite amplitude chorus. The effect of the nonlinear frequency and wave number shifts due to an incremental change in the fluctuation spectrum is discussed in Section 4. Meanwhile, ω and k in Equations 30 and 31 are interpreted as elements of the whistler fluctuation spectrum that is considered dense (nearly continuous) and is self-consistently evolving in time as a whole in the presence of the hot electron free energy source (Tao et al., 2020; Zonca et al., 2017), rather than considered as properly chosen "whistler seeds" that are representative of the selected chorus element (Omura & Nunn, 2011). This is one of the main differences of the present work with respect to the earlier analysis by Omura and Nunn (2011), as discussed in Section 1. The other one consists in the analytic solution for the self-consistent nonlinear hot electron response in phase space (Tao et al., 2020; Zonca et al., 2017), which is discussed below. Section 4 also allows us to reconcile different interpretations of chorus chirping (Omura & Nunn, 2011)) inside the same framework with a self-consistent comprehensive vision and to address some of the issues regarding subelements as presented in the recent work by Tsurutani et al. (2020).

When

$$\delta\hat{\bar{f}}_k = \mathcal{L}_k^{-1}\left\{\frac{e}{m}v_\perp\delta\bar{E}_k\left[\frac{k}{\omega}\frac{\partial}{\partial v_\parallel}+\left(1-\frac{kv_\parallel}{\omega}\right)\frac{1}{v_\perp}\frac{\partial}{\partial v_\perp}\right]\hat{f}_0\right\} \quad (32)$$

is substituted back into Equation 30, the "formal solution" for $\hat{f}_0$ is obtained and can be cast in the form of a Dyson-like equation (Dyson, 1949; Itzykson & Zuber, 1980; Schwinger, 1951)

$$\begin{aligned}(\partial_t + v_\parallel\partial_z)\,\hat{f}_0 \;=\; & \frac{1}{4}\sum_k i\frac{e}{m}v_\perp\delta\bar{E}_k\left[\frac{k}{\omega}\frac{\partial}{\partial v_\parallel}+\left(1-\frac{kv_\parallel}{\omega}\right)\left(\frac{1}{v_\perp}\frac{\partial}{\partial v_\perp}+\frac{1}{v_\perp^2}\right)\right]\\ & \times\mathcal{L}_k^{*-1}\left\{\frac{e}{m}v_\perp\delta\bar{E}_k^*\left[\frac{k}{\omega}\frac{\partial}{\partial v_\parallel}+\left(1-\frac{kv_\parallel}{\omega}\right)\frac{1}{v_\perp}\frac{\partial}{\partial v_\perp}\right]\hat{f}_0\right\}\\ & -\frac{1}{4}\sum_k i\frac{e}{m}v_\perp\delta\bar{E}_k^*\left[\frac{k}{\omega}\frac{\partial}{\partial v_\parallel}+\left(1-\frac{kv_\parallel}{\omega}\right)\left(\frac{1}{v_\perp}\frac{\partial}{\partial v_\perp}+\frac{1}{v_\perp^2}\right)\right]\\ & \times\mathcal{L}_k^{-1}\left\{\frac{e}{m}v_\perp\delta\bar{E}_k\left[\frac{k}{\omega}\frac{\partial}{\partial v_\parallel}+\left(1-\frac{kv_\parallel}{\omega}\right)\frac{1}{v_\perp}\frac{\partial}{\partial v_\perp}\right]\hat{f}_0\right\}.\end{aligned} \quad (33)$$

Connections of the present approach with the field theoretical description based on the Dyson-Schwinger equations are extensively analyzed in Chen and Zonca (2016) and Zonca et al. (2015b) as far as magnetized fusion plasma applications are concerned. Interested readers may find the same analyses specialized to chorus wave excitation in Appendix B. Here, we emphasize that the general theoretical framework (Aamodt, 1967; Al'Tshul' & Karpman, 1966; Balescu, 1963; Chen & Zonca, 2016; Dupree, 1966; Mima, 1973; Prigogine, 1962; van Hove, 1954; Weinstock, 1969; Zonca et al., 2015a, 2015b, 2017) is of crucial importance for demonstrating that Equations 32 and 33 do indeed account for the phase-space structures that determine the dominant nonlinear dynamics and phase space transport by chorus emission. In fact, the dynamic description given by Equation 33 accounts for phase space nonlinear behaviors without fast temporal or spatial dependences, which correspond to the self-interaction of the fluctuation with the wavenumber of interest with itself. The resultant distortion of the hot electron distribution function, determined self-consistently in the presence of the finite amplitude fluctuation spectrum, constitutes the "renormalized" hot electron response of interest for the present application. Solving Equation 33 together with the wave equations, Equations 11 and 14, preserves the crucial underlying physics of chorus nonlinear evolution but is beyond the scope of the present work. Here, we focus on chorus frequency chirping rather than on the details of phase space nonlinear dynamics and transport. Thus, in the next section, we introduce a reduced (velocity space averaged) description of the Dyson-like equation that will allow us to derive nonlinear evolution equations for $\bar{W}(z,t,\omega)$ and $\bar{\Gamma}(z,t,\omega)$ and, thereby, analytically address the dynamics of chorus chirping.

3. Reduced Dyson-Like Equation

Let us reconsider the simplified expressions of $\bar{W}(z,t,\omega)$ and $\bar{\Gamma}(z,t,\omega)$, Equation 27, obtained in Section 2.2. On the right-hand side, formally consider. $\hat{f}_0 \equiv (\partial_t + v_\parallel\partial_z)^{-1}(\partial_t + v_\parallel\partial_z)\,\hat{f}_0$ and use Equation 33 for the expression of $(\partial_t + v_\parallel\partial_z)\,\hat{f}_0$. In other words, we formally manipulate the Dyson-like equation obtained in Section 2.2 and integrate in velocity space in order to obtain reduced expressions for time evolving $\bar{W}(z,t,\omega)$ and $\bar{\Gamma}(z,t,\omega)$ rather than solving Equation 33 in the whole phase space (Tao et al., 2020; Zonca et al., 2017). This reduced approach becomes useful when the nonlinear particle response is dominated by resonant particles in the presence of a quasi-coherent (narrow) wave packet such as in the case of chorus. The same approach has been successfully applied to study energetic particle modes (Zonca et al., 2015b) as well as the so-called "fishbone" mode (Chen & Zonca, 2016) in fusion plasmas. Let us also recall the approximation introduced at the beginning of Section 2.2, by which we assume that hot electrons are a nonuniform source localized about the equator, while the remaining dynamics is well described neglecting magnetic field nonuniformity. Thus, Equation 23 gives $T_\omega(z) \simeq z/v_{g\omega}$ and $T_\omega^{-1}(t) \simeq v_{g\omega}t$. Furthermore, at any position z sufficiently outside the localized nonuniform hot electron source, $I(z, t, \omega)$ and $\varphi(z,t,\omega)$ are predominantly functions of $t - z/v_{g\omega}$, as can be verified from Equations 22 and 24 computing ∂_t and ∂_z of those expressions. Repeating the same argument, predominant dependence on $t - z/v_{g\omega}$ can be demonstrated for $\hat{f}_0$, $\bar{W}$, and $\bar{\Gamma}$. Residual z dependences are neglected, since they account for magnetic field nonuniformity, which is omitted here for simplicity, and modulation effects of the chorus wave packet due to the finite extent of the source region. These effects are reported in detailed numerical investigations by Wu et al. (2020), illustrating the role of magnetic field nonuniformity in breaking the symmetry between rising and falling tone chorus. In more recent work (Tao et al., 2021), chorus nonlinear dynamics due to wave-particle interactions and magnetic field nonuniformity have been analyzed on the same footing within a newly developed phenomenological "TaRA model," as anticipated in Section 1. The present simplified theoretical description reduces the dimensionality of the problem and allows us to adopt useful simplifications; e.g., $(\partial_t + v_\parallel\partial_z) \simeq (1 - v_{r\omega}/v_{g\omega})\partial_t$ when dealing with resonant particles. Numerical studies of the complete Dyson-like Equation 33 will be given elsewhere.

Based on these assumptions, on the right-hand side of Equation 33 we can write

$$i\left(\delta\bar{E}_k\mathcal{L}_k^{*-1}\delta\bar{E}_k^* - \delta\bar{E}_k^*\mathcal{L}_k^{-1}\delta\bar{E}_k\right) = i\left(\delta\bar{E}_k\mathcal{L}_k^{*-1}\mathcal{L}_k^{-1}\mathcal{L}_k\delta\bar{E}_k^* - \delta\bar{E}_k^*\mathcal{L}_k^{-1}\mathcal{L}_k^{*-1}\mathcal{L}_k^*\delta\bar{E}_k\right). \tag{34}$$

Noting

$$\mathcal{L}_k^{*-1}\mathcal{L}_k^{-1} \simeq \mathcal{L}_k^{-1}\mathcal{L}_k^{*-1} \simeq \left[\mathcal{L}_k\mathcal{L}_k^*\right]^{-1} = \left[(\Omega_e + kv_\parallel - \omega)^2 + (1 - v_{r\omega}/v_{g\omega})^2\partial_t^2\right]^{-1}, \tag{35}$$

where, again, the notation $[\ldots]^{-1}$ always denotes the inverse of an operator within the square brackets, Equation 34 can be cast as

$$\begin{aligned} i\left(\delta\bar{E}_k\mathcal{L}_k^{*-1}\delta\bar{E}_k^* - \delta\bar{E}_k^*\mathcal{L}_k^{-1}\delta\bar{E}_k\right) &= i\Big\{\delta\bar{E}_k\left[(\Omega_e + kv_\parallel - \omega)^2 + (1 - v_{r\omega}/v_{g\omega})^2\partial_t^2\right]^{-1}\mathcal{L}_k\delta\bar{E}_k^* \\ &\quad - \delta\bar{E}_k^*\left[(\Omega_e + kv_\parallel - \omega)^2 + (1 - v_{r\omega}/v_{g\omega})^2\partial_t^2\right]^{-1}\mathcal{L}_k^*\delta\bar{E}_k\Big\} \\ &\simeq 2|\delta\bar{E}_k|\left[(\Omega_e + kv_\parallel - \omega)^2 + (1 - v_{r\omega}/v_{g\omega})^2\partial_t^2\right]^{-1} \\ &\quad \times(1 - v_{r\omega}/v_{g\omega})\partial_t|\delta\bar{E}_k|. \end{aligned} \tag{36}$$

Here, as it can be verified by inspection, the operators action on the phase dependences in $\delta\bar{E}_k = |\delta\bar{E}_k|e^{i\varphi}$ and its complex conjugate cancel each other and only $(1 - v_{r\omega}/v_{g\omega})\partial_t|\delta\bar{E}_k|$ survives. Using this expression and substituting Equation 33 back into Equation 27, we finally obtain, after tedious but straightforward algebra (cf. Appendix C1)

$$\begin{aligned} \bar{W}(\bar{\omega}) + i\bar{\Gamma}(\bar{\omega}) &= \frac{n_e}{n}\left(1 - \frac{v_{r\bar{\omega}}}{v_{g\bar{\omega}}}\right)^2\Bigg\langle\frac{v_\perp^4}{2}\Omega_e\left[\Omega_e + \bar{k}v_\parallel - \bar{\omega} - i(1 - v_{r\bar{\omega}}/v_{g\bar{\omega}})\partial_t\right]^{-1} \\ &\quad \times\left(\frac{\bar{k}}{\bar{\omega}}\frac{\partial}{\partial v_\parallel} - \frac{2}{\langle v_\perp^2\rangle}\frac{\Omega_e}{\bar{\omega}}\right)(\partial_t + v_\parallel\partial_z)^{-1}\sum_k\frac{e^2}{2m^2}|\delta\bar{E}_k|\frac{k}{\omega}\frac{\partial}{\partial v_\parallel} \\ &\quad \times\left[(\Omega_e + kv_\parallel - \omega)^2 + (1 - v_{r\omega}/v_{g\omega})^2\partial_t^2\right]^{-1}(1 - v_{r\omega}/v_{g\omega}) \\ &\quad \times\partial_t|\delta\bar{E}_k|\left(\frac{k}{\omega}\frac{\partial}{\partial v_\parallel} - \frac{2}{\langle v_\perp^2\rangle}\frac{\Omega_e}{\omega}\right)\hat{f}_0\Bigg\rangle. \end{aligned} \tag{37}$$

Here, we have repeatedly integrated by parts in $v_\perp$, from outside to the inside, in order to remove any $\partial/\partial v_\perp$ in the final expression. Moreover, for simplicity of notation, we have explicitly indicated only the frequency dependence of $\bar{W}$ and $\bar{\Gamma}$, leaving implicit the dependence on $t - z/v_{g\bar{\omega}}$. Finally $\langle v_\perp^2 \rangle \equiv \langle v_\perp^2 \hat{f}_0 \rangle / \langle \hat{f}_0 \rangle$, and we have denoted the current frequency and wave number satisfying the lowest order whistler wave dispersion relation as $\bar{\omega}$ and $\bar{k}$ in order to distinguish them from ω and k in the running summation over the fluctuation spectrum.

Equation 37 still contains all the information embedded in the solution of the Dyson-like equation, Equation 33, via complicated integro-differential operators. In order to make further progress, we explicitly carry out the velocity space integration adopting two assumptions: (a) the chorus spectrum is narrow, such that $(\omega, k) \simeq (\bar{\omega}, \bar{k})$ and $\partial_t|\delta\bar{E}_k| \simeq \partial_t|\delta\bar{E}_{\bar{k}}|$; (b) chorus chirping is due to the subsequent emission of different waves belonging to the whistler wave continuum, which are excited in turns to maximize wave particle power transfer. The assumption (b) was already introduced in the remarks following Equation 33 in Section 2.2 and will be further discussed below in Section 4. Meanwhile, both assumptions are based on the chorus spectral features and are the same as those of fluctuation spectra in the aforementioned fusion applications (Chen & Zonca, 2016; Zonca et al., 2015b). After tedious but straightforward algebra, some details of which are reported in Appendix C2 for interested readers, real and imaginary parts of Equation 37 can be cast as

$$\begin{aligned} \Omega_e^{-1}\partial_t \bar{W}(\bar{\omega}) \quad = \quad & \left[\Omega_e \frac{\partial}{\partial\bar{\omega}} - \frac{2\Omega_e^2}{\bar{k}^2 \langle v_\perp^2 \rangle} \left(1 - \frac{v_{r\bar{\omega}}}{v_{g\bar{\omega}}} \right) \right] \Omega_e \frac{\partial}{\partial\bar{\omega}} \\ & \times \sum_k \frac{(\omega - \bar{\omega})}{2\Omega_e} \left[\frac{(\omega - \bar{\omega})^2}{4\Omega_e^2} + \Omega_e^{-2}\partial_t^2 \right]^{-1} \\ & \times \frac{\langle\langle \omega_{\mathrm{tr}k}^4 \rangle\rangle}{4\Omega_e^4 (1 - v_{r\omega}/v_{g\omega})^4} \left(\frac{\bar{\Gamma}(\omega) + \bar{\Gamma}(\bar{\omega})}{2} \right); \end{aligned} \tag{38}$$

and, denoting as $\bar{\Gamma}_L$ the linear (initial) normalized hot electron driving rate

$$\begin{aligned} \bar{\Gamma}(\bar{\omega}) - \bar{\Gamma}_L(\bar{\omega}) \quad = \quad & \left[\Omega_e \frac{\partial}{\partial\bar{\omega}} - \frac{2\Omega_e^2}{\bar{k}^2 < v_\perp^2 >} \left(1 - \frac{v_{r\bar{\omega}}}{v_{g\bar{\omega}}} \right) \right] \Omega_e \frac{\partial}{\partial\bar{\omega}} \\ & \times \sum_k \left[\frac{(\omega - \bar{\omega})^2}{4\Omega_e^2} + \Omega_e^{-2}\partial_t^2 \right]^{-1} \\ & \times \frac{<< \omega_{\mathrm{tr}k}^4 >>}{4\Omega_e^4 (1 - v_{r\omega}/v_{g\omega})^4} \left(\frac{\bar{\Gamma}(\omega) + \bar{\Gamma}(\bar{\omega})}{2} \right), \end{aligned} \tag{39}$$

where we have introduced the wave particle trapping frequency definition

$$\langle\langle \omega_{\mathrm{tr}k}^4 \rangle\rangle \equiv \langle v_\perp^2 \omega_{\mathrm{tr}k}^4 \hat{f}_0 \rangle / \langle v_\perp^2 \hat{f}_0 \rangle, \tag{40}$$

with $\omega_{\mathrm{tr}k}^2 = |(e/m)k^2 v_\perp \delta\bar{E}_k/\omega|$.

Equations 38 and 39 are still complicated nonlinear integro-differential equations, but they have been significantly simplified (or reduced) with respect to the original Dyson-like equation, Equation 33. These equations are the primary theoretical results of the present work and show that $\bar{W}$ and $\bar{\Gamma}$ evolution equations are interlinked as expected and as anticipated in Section 2.1. They describe a variety of nonlinear dynamics, including chorus chirping and modulation of the chorus wave packets on a time scale $\sim \langle\langle \omega_{\mathrm{tr}k}^4 \rangle\rangle^{-1/4}$. To see this more clearly, let us introduce the optimal ordering for Equations 38 and 39. The width of the fluctuation spectrum can be estimated as

$$\frac{|\omega - \bar{\omega}|}{2\Omega_e} \sim \frac{\partial_t \bar{W}}{\Omega \bar{\Gamma}_{NL}}. \tag{41}$$

Meanwhile, assuming $|\partial_{\bar{\omega}}^2 \Gamma_{NL}| \gtrsim |\partial_{\bar{\omega}}^2 \Gamma_L|$, ordering all terms of Equation 39 on the same footing gives

$$|\partial_t| \sim |\omega - \bar{\omega}| \sim |\partial_{\bar{\omega}}|^{-1} \sim \langle\langle \omega_{\mathrm{tr}k}^4 \rangle\rangle^{1/4} \sim \hat{\gamma}_e, \tag{42}$$

where $\hat{\gamma}_e$ is the peak value of the linear hot electron driving rate at the equator. Equation 42 describes a whistler wave packet that grows and saturates locally due to wave particle trapping. However, if chirping consistent with

Equation 1 sets in as in chorus spontaneous emission, saturation at the level of Equation 42 is not possible and the wave packet can grow further. Equation 39, then, suggests

$$|\partial_t| \sim \left\langle\left\langle \omega_{\mathrm{tr}k}^4 \right\rangle\right\rangle^{1/2} |\partial_{\bar\omega}| \sim \frac{\left\langle\left\langle \omega_{\mathrm{tr}k}^4 \right\rangle\right\rangle^{1/2}}{|\omega - \bar\omega|} \gtrsim |\omega - \bar\omega| \,. \tag{43}$$

This ordering corresponds to a characteristic nonlinear time, $\tau_{NL} \sim |\partial_t|^{-1} \sim \Gamma_{NL}^{-1}$ that is shorter than the wave particle autocorrelation time, $|\Delta\omega|^{-1} \sim |\omega - \bar\omega|^{-1}$. In particular, this ordering is consistent with chorus chirping, and Equation 39 readily yields Equation 1 when we assume a quasi-coherent (nearly monochromatic) fluctuation spectrum. In fact, keeping the leading terms only in Equation 39, consistent with Equation 43, we have that $\Omega_e^{-2}\partial_t^2$ dominates in the integral operator definition, Equation 39, and

$$\frac{\partial^2}{\partial t^2}\bar\Gamma_{NL}(\bar\omega) \simeq \left(\sum_k \frac{\left\langle\left\langle \omega_{\mathrm{tr}k}^4 \right\rangle\right\rangle}{4(1 - v_{r\omega}/v_{g\omega})^4} \right) \frac{\partial^2}{\partial\bar\omega^2}\bar\Gamma_{NL}(\bar\omega). \tag{44}$$

This result suggests that there exists a self similar solution for $\bar\Gamma_{NL}$ that ballistically propagates in ω-space at a rate given by the square root of the quantity in square parentheses on the right-hand side. This ballistic propagation corresponds to the analogous ballistic propagation of hot electron phase-space structures, described by Equation 33; and it is in one-on-one correspondence with the analogous ballistic propagation of phase space zonal structures connected with energetic particle avalanches in fusion plasmas (Chen & Zonca, 2016; Zonca et al., 2015b). Details obviously depend on the actual form of the spectrum, but it is readily verified that, for nearly monochromatic chorus element, Equation 44 yields

$$\frac{\partial\omega}{\partial t} = \pm\frac{1}{2}\frac{\left\langle\left\langle \omega_{\mathrm{tr}k}^4 \right\rangle\right\rangle^{1/2}}{(1 - v_{r\omega}/v_{g\omega})^2}. \tag{45}$$

Thus, the present theoretical framework is consistent with both upward and downward frequency sweeping of chorus structures and, thus, consistent with the recent work by Wu et al. (2020). This is the first theoretical prediction for the downward chirping of parallel propagating waves, as far as we are aware of. However, it should also be noted that statistical observations of chorus falling tones show that they are mainly very oblique rather than parallel (Li et al., 2011), and that Mourenas et al. (2015) have predicted the possible existence of both positive and negative frequency chirping for such very oblique chorus waves based on the maximization of the nonlinear growth rate of Shklyar and Matsumoto (2011). More detailed discussions on the chirping direction will be given below in Section 4. Focusing, here, on the positive sign of Equation 45, by direct inspection it can be noted that it coincides with Equation 1 for $R = 1/2$ as anticipated in Section 1 (Vomvoridis et al., 1982). Equation 45 improves an earlier estimate by the same authors (Zonca et al., 2017) and, to our knowledge, is the first self-consistent analytical demonstration of the conjecture by Vomvoridis et al. (1982) in its exact initial formulation. More generally, Equation 44 suggests why the chorus chirping rate is not always given by $R = 1/2$, the limiting case for a nearly monochromatic spectrum, but may vary depending on the excitation conditions; e.g., the initial hot electron distribution function.

4. On Chorus Chirping

In order to further illuminate the features of chorus dynamics as predicted by Equations 38 and 39, we have solved them numerically, together with the wave equations of Section 2.1, using a fourth-order Runge-Kutta method. To exploit the dense nature of the whistler wave spectrum, we introduce the dimensionless intensity $\mathcal{I}(\omega)$ such that nonlinearity effects become important when $\mathcal{I}(\omega) \sim \mathcal{O}(1)$ (cf. Appendix D).

Assuming fixed $z\Omega_e/c = 50$ and parameters as in Figure 1, the nonlinear evolution of $\mathcal{I}(z = 50c/\Omega_e, t, \omega)$ is shown in Figure 3. Here, rather than assuming a specific form of the initial spectrum, we assumed vanishing initial conditions and a constant slow external stirring that, in the absence of suprathermal electrons, would give an intensity spectrum $\mathcal{I} = \mathcal{S}^2\Omega_e^2 t^2$, corresponding to $|\delta \bar E_k|$ linearly increasing with time (cf. Appendix D). In Figure 3, the source strength is $\mathcal{S} = 2 \times 10^{-5}$. Furthermore, we use a discretization in ω space with 221 grid points in the interval $\omega/\Omega_e \in [0.05, 0.9]$ and adopt a Savitzky-Golay filter fitting subsets of 19 adjacent data points with

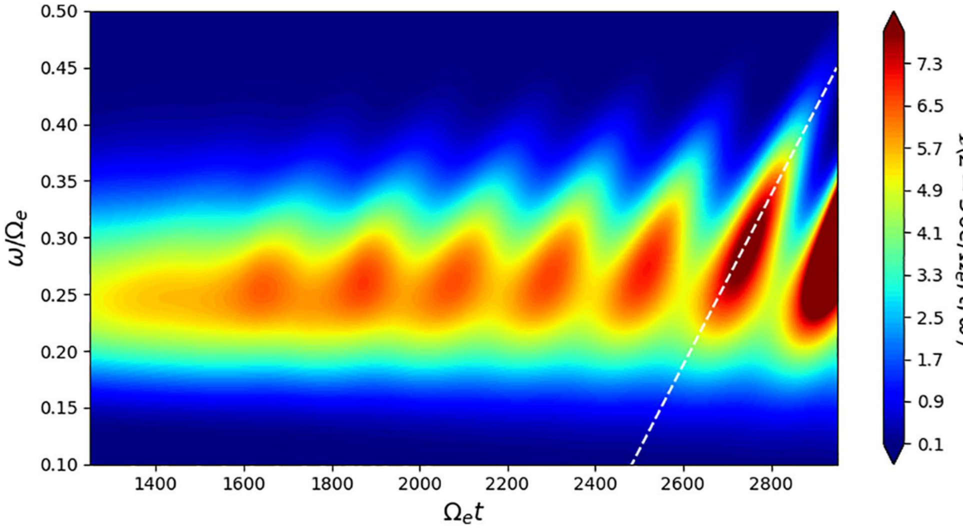

Figure 3. Contour plot of the nonlinear evolution of $\mathcal{I}(\omega)$ for a uniform source $\mathcal{S} = 2 \times 10^{-5}$ in Equation D5. The position is fixed at $z\Omega_e/c = 50$ and parameters are the same as in Figure 1. The white dashed line passing through the chorus element beginning at $\Omega_e t \sim 2{,}600$ represents the average chirping rate $\partial_t \omega_0 = 7.5 \times 10^{-4} \Omega_e^2$.

a fourth-order degree polynomial to ensure regularity of the derivatives in ω-space. A fourth-order Runge-Kutta integration in time is adopted with variable time step, gradually decreasing from an initial $\Omega_e \Delta t = 1.25 \times 10^{-1}$ in the early linear evolution to $\Omega_e \Delta t = 3.125 \times 10^{-2}$ in the later nonlinear phase at $\Omega_e t > 1{,}750$. This choice ensures that Courant condition is well satisfied. The routine solving Equations D2–D6, closed by Equations D7 and D8, together with the proper boundary conditions, is written in Python and uses Python standard libraries. In order to illustrate the robustness of the present numerical results as parameters are varied, Figure 4 shows the nonlinear evolution of $\mathcal{I}(z = 50c/\Omega_e, t, \omega)$ for $\mathcal{S} = \sqrt{2} \times 10^{-5}$ and same physical parameters of Figure 3. In this case, the Savitzky-Golay filter is reduced to fitting subsets of 15 adjacent data points with a fourth-order degree polynomial.

Various distinctive features clearly emerge in Figures 3 and 4. After the initial formation of the "linear" fluctuation spectrum, clear modulations at the $\left\langle\left\langle \omega_{\rm trk}^4 \right\rangle\right\rangle^{1/4}$ frequency become increasingly more evident as the fluctuation intensity $\mathcal{I}$ grows larger than unity, as expected from the previous theoretical analysis and from Tao

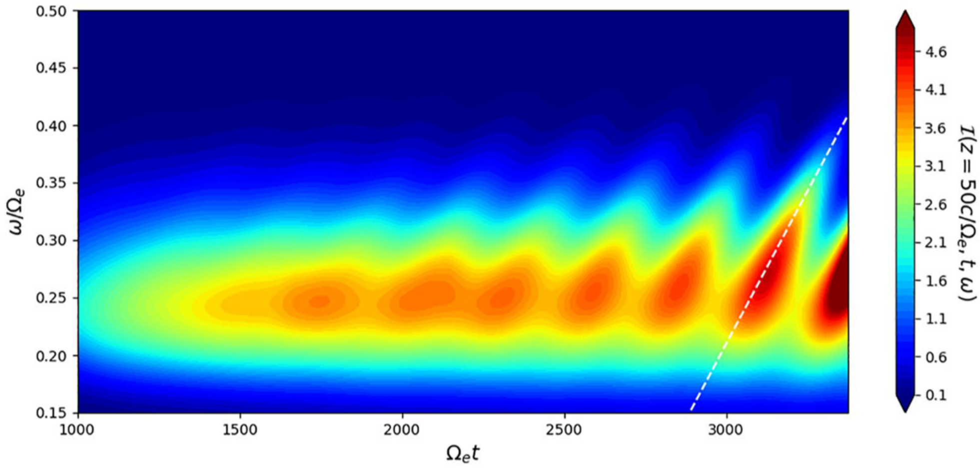

Figure 4. Contour plot of the nonlinear evolution of $\mathcal{I}(\omega)$ for a uniform source $\mathcal{S} = \sqrt{2} \times 10^{-5}$ in Equation D5. As in Figure 3, the position is fixed at $z\Omega_e/c = 50$ and parameters are the same as in Figure 1. The white dashed line passing through the chorus element beginning at $\Omega_e t \sim 3{,}000$ represents the average chirping rate $\partial_t \omega_0 = 5.3 \times 10^{-4} \Omega_e^2$ as obtained from particle-in-cell (PIC) simulation by the DAWN code in Tao et al. (2017a).

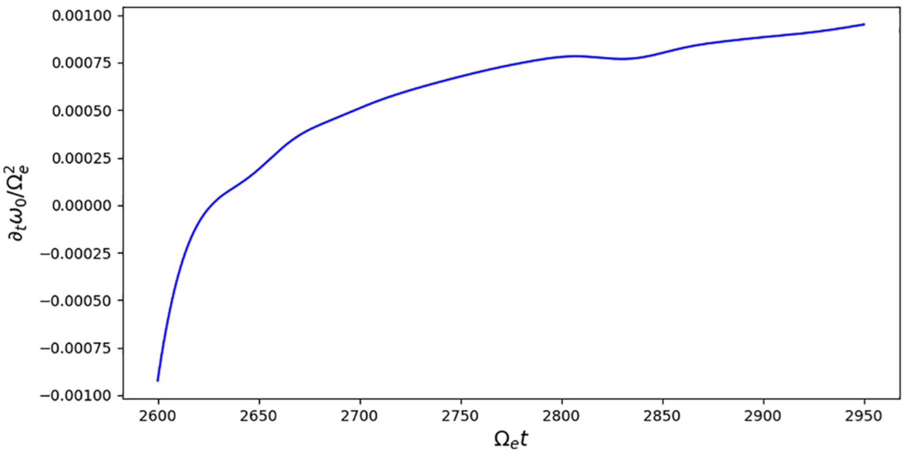

Figure 5. Instantaneous chirping rate of the intensity peak of the rising tone chorus element beginning at $\Omega_e t \sim 2{,}600$ in Figure 3.

et al. (2017a). Note that these modulations are different from the amplitude modulations within one chorus element leading to the so-called "subpackets" or "subelements" (Santolík et al., 2003). However, they stem from the same physics; i.e., the spectrum intensity modulation due to the finite frequency width of the wave packet as shown in Equation D2. Nonlinear oscillations, as intensity increases, are accompanied by gradually increasing frequency chirping, which can be both up or down. This behavior is consistent with Equation 45 and, despite no clear falling tone chorus element is observed here, it is also consistent with the recent numerical investigation by Wu et al. (2020). Further strengthening of the nonlinear oscillations due to the continuous energy injection in the system by the uniform source $\mathcal{S}$, which is amplified via resonant wave particle power exchange and structure formation in the phase space, breaks the up-down symmetry in the chirping process because of the lack of symmetry (in frequency) of the linear drive about its maximum (cf. Figure 1) and because of the symmetry breaking term in the first line on the right-hand side of Equation D3. Another origin of symmetry breaking in frequency chirping is due to the nonuniformity due to the ambient magnetic field (Wu et al., 2020), which, however, is neglected for the sake of simplicity in the present theoretical analysis. Focusing on the rising tone chorus element beginning at $\Omega_e t \sim 2{,}600$ in Figure 3, the frequency chirping is well represented by Equation 45 and is fitted by the average chirping rate $\partial_t\omega_0 = 7.5 \times 10^{-4}\Omega_e^2$. For the somewhat weaker power injection in Figure 4, the chirping of rising tone chorus element beginning at $\Omega_e t \sim 3{,}000$ agrees remarkably well with the average chirping rate $\partial_t\omega_0 = 5.3 \times 10^{-4}\Omega_e^2$ as obtained from PIC simulation by the DAWN code in Tao et al. (2017a) and, again, is visually given by the white dashed line. The average chirping rate dependence on the fluctuation intensity further confirms Equation 45. The average chirping rate is also confirmed by the instantaneous chirping rate of the intensity peak given in Figure 5. Noting $\partial_t\omega_0/\Omega_e^2$ is starting from negative values, as noted above, is consistent with the possibility of both up-chirping and down-chirping and, thus, with Equation 45. However, here, we cannot observe a clear formation of a falling tone chorus element unlike in Wu et al. (2020), despite the evidence of initial down-chirping. As the rising tone chorus element is clearly formed with the corresponding phase-space structure, the chirping rate reaches up to its average value as visually suggested by the white dashed line in Figure 3. Time evolution of intensity peak $\mathcal{I}_0(z = 50c/\Omega_e, t)$ and corresponding phase shift $\Delta\varphi_0(z = 50c/\Omega_e, t)$ for this chorus element are given in Figure 6 and further clarify the underlying physics. An important conclusion we may draw from Figure 6 is that intensity grows while $\Delta\varphi_0 \simeq 0$; i.e., during phase locking. This behavior is due to phase bunching of both trapped and untrapped resonant particles, which most effectively drive the chorus wave packet. The same behavior allows us drawing strong connection with the analogous behavior of energetic particle avalanches in fusion plasmas (Chen & Zonca, 2016; Zonca et al., 2015b). Meanwhile, the intensity peak takes place when $\Delta\varphi_0 = \pi$ and resonant particles phase locking is lost yielding the end of the chorus event. This mechanism can be viewed as the chorus wave packet slipping over the population of resonant electrons maximizing wave particle power extraction, and suggests the analogy with superradiance in free electron lasers introduced by Zonca et al. (2015b) and Chen and Zonca (2016) with regard to energetic particle mode convective amplification in fusion plasmas. Analogies with the free electron laser were also noted by numerical simulation studies in Soto-Chavez et al. (2012). That it is indeed maximization of wave particle power transfer (Chen & Zonca, 2016;

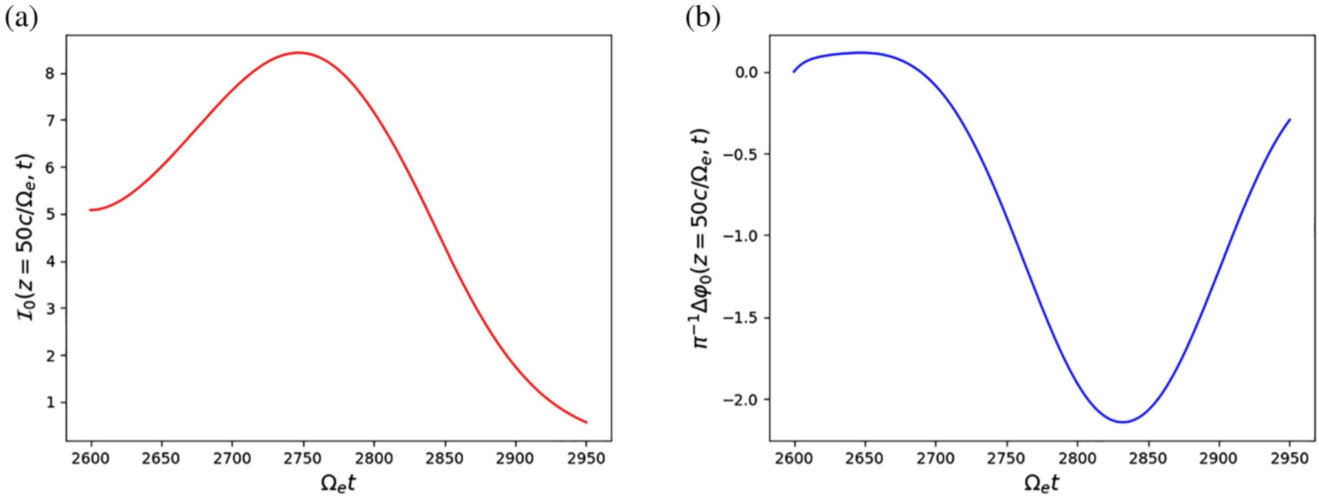

Figure 6. Time evolution of intensity peak $\mathcal{I}_0(z = 50c/\Omega_e, t)$ (a) and corresponding phase shift $\Delta\varphi_0(z = 50c/\Omega_e, t)$ (b) for the rising tone chorus element beginning at $\Omega_e t \sim 2{,}600$ in Figure 3.

Omura et al., 2008; Vomvoridis et al., 1982; Zonca et al., 2015a, 2015b) that dictates the nonlinear chorus dynamics and frequency chirping is further demonstrated by Figure 7. Figure 7a shows that the nonlinear frequency shift, $\Delta_\omega(z = 50c/\Omega_e, t)$, remains small during the whole nonlinear evolution and, in particular, much smaller than the dynamic range of frequency chirping, consistent with the assumption that each elementary wave constituting the chorus wave packet satisfies the whistler wave dispersion relation at the lowest order. Figure 7b, meanwhile, shows a snapshot of $\Delta_\omega(z = 50c/\Omega_e, t = 2{,}875/\Omega_e)$. By definition, at the intensity peak the wave particle power transfer is maximized; and, since the chirping process is spontaneously triggered by the underlying instability, the nonlinear evolution follows the maximum possible intensity growth or minimum possible intensity decrease. In fact, it is important to recognize that power transfer is maximized even in the intensity decreasing phase (Chen & Zonca, 2016; Zonca et al., 2015a, 2015b). Another aspect that is clarified by the present approach and is the issue of "subpackets" or "subelements" (Santolík et al., 2003) formation within a single chorus element. While Figures 3 and 4 display the spectrum intensity only, Figure 8 illustrates the temporal structure of the perpendicular magnetic field fluctuation, $|\delta \boldsymbol{B}_\perp|/B_e$, reconstructed from Equations 7 and 9, for the rising tone chorus element beginning at $\Omega_e t \sim 2{,}600$ in Figure 3. The formation of subelements is clear, qualitatively, and quantitatively consistent with the PIC simulation by the DAWN code done with the same parameters in Tao et al. (2017a).

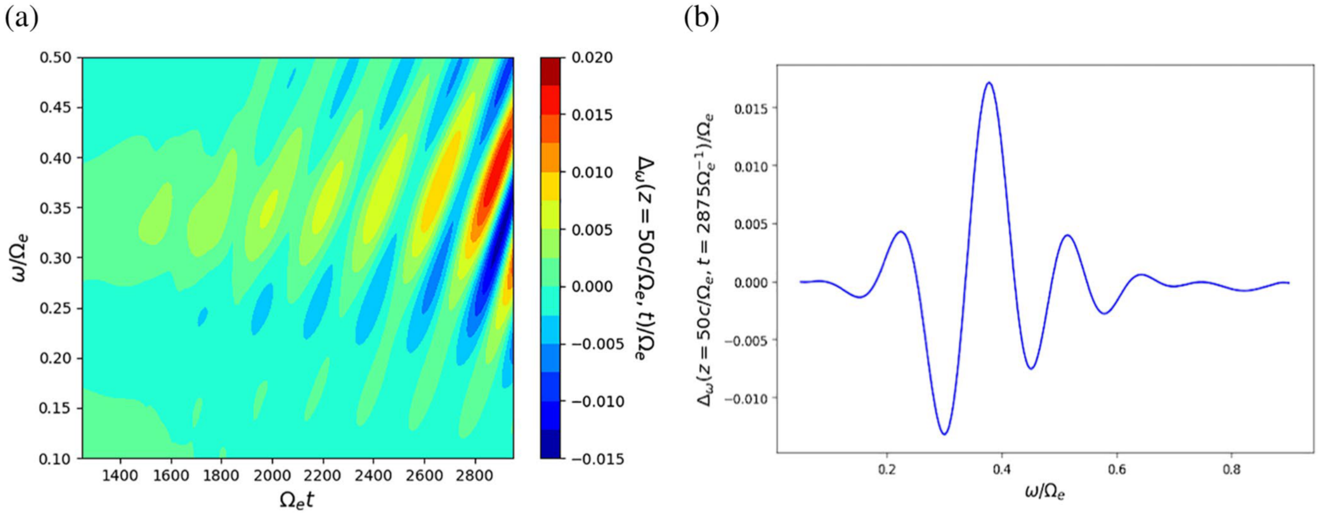

Figure 7. Contour plot of the nonlinear frequency shift, $\Delta_\omega(z = 50c/\Omega_e, t)$ (a) and snapshot of $\Delta_\omega(z = 50c/\Omega_e, t = 2{,}875/\Omega_e)$ (b).

10.1029/2021JA029760

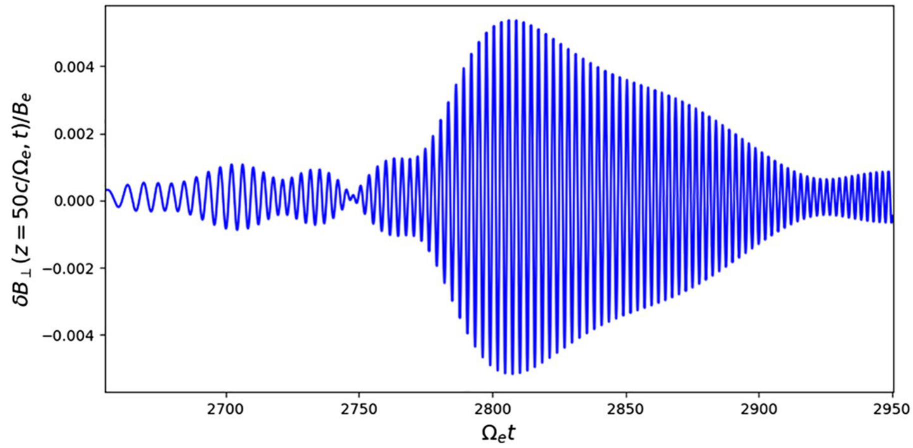

Figure 8. Temporal structure of the perpendicular magnetic field fluctuation, $|\delta \boldsymbol{B}_{\perp}|/B_e$ for the rising tone chorus element beginning at $\Omega_e t \sim 2{,}600$ in Figure 3. Formation of "subpackets" or "subelements" (Santolík et al., 2003) is clearly illustrated.

This evidence supports the corresponding original interpretation provided therein that chorus subelement formation is to be attributed to the phase modulation and "self-consistent evolution of resonant particle phase-space structures and spatiotemporal features of the fluctuation spectrum," proposed by O'Neil (1965) when analyzing collisionless damping of nonlinear plasma oscillations. These results also clarify that nonlinear oscillations are connected with the width of the fluctuation intensity spectrum and stem from the same underlying physics, as noted above. In close connection and consistent with the present analysis, it is important to quote the recent statistical results from Zhang et al. (2020) on observed typical wave packet lengths, amplitudes, and frequency variations of rising tone chorus elements. Short packets have been explained by Zhang et al. (2020) and Nunn et al. (2021) as resulting from trapping-related amplitude modulations for packets longer than about 10 wave periods, and as a result of wave superposition of two well-separated waves sensibly farther than a trapping period for shorter packets. Formation of subpackets in chorus emission was also recently analyzed by Hanzelka et al. (2020) adopting the sequential triggering model by Omura and Nunn (2011).

Given the present theoretical analysis and numerical solutions, the explanation of chorus frequency chirping given by Omura and Nunn (2011) may seemingly be in contrast with the present results. As anticipated in Section 1, the reason for frequency chirping was explained as due to the nonlinear current parallel to the wave magnetic field (J_B), which causes a nonlinear frequency shift. More precisely, the physics mechanism underlying chirping is the sequence of "whistler seeds" that are excited and amplified by wave particle resonant interactions with suprathermal electrons. In the present work, the fluctuation spectrum is self-consistently evolved out of a very weak "white spectrum" source. Each oscillator in the wave spectrum can be characterized by a small nonlinear frequency shift (cf. Figure 7). However, the wave packet that spontaneously evolves from the superposition of these oscillators sweeps upward in frequency to maximize wave particle power exchange. While doing so, self-consistency between chirping and rate of change of nonlinear frequency shift should be "locked." This is visible in Figure 9a where the intensity peak frequency (blue line) of the chorus element considered in Figure 3 is compared with the frequency of the corresponding peak of the rate of change of nonlinear frequency shift (red line). Recalling the discussion preceding Equation D7, the rate of change of the resonant frequency is $\partial_t \omega_{\rm res} = (1 - v_{r\omega}/v_{g\omega})\partial_t \Delta_\omega$. A snapshot at $\Omega_e t = 2{,}875$ of the fluctuation intensity and of the $\partial_t \omega_{\rm res}$ as a function of frequency is given in Figure 9b. Thus, interpreting the "whistler seeds" of Omura and Nunn (2011) as the swinging oscillators in the wave packet at the intensity peak, one should obtain the frequency increase due to the chorus chirping as

$$\Delta\omega = \int (1 - v_{r\omega_0(t')}/v_{g\omega_0(t')})\partial_{t'} \Delta_{\omega_0(t')} dt',$$

where integration is to be intended along the red line of Figure 9a. The hence obtained frequency increase is $\Delta\omega/\Omega_e = 0.24$ over the considered time interval, against the corresponding frequency shift $\Delta\omega/\Omega_e = 0.21$ of the intensity peak. Such a good agreement confirms the present explanation that reconciles the original interpretation of frequency chirping given by Omura and Nunn (2011) with the present theoretical analysis.

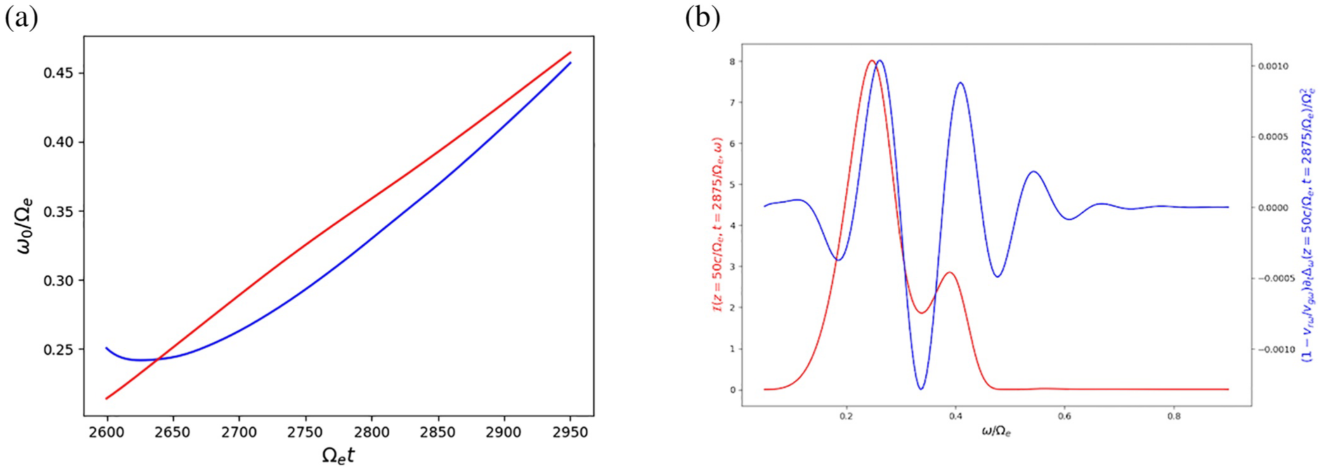

Figure 9. (a) Time evolution of intensity peak frequency (blue line) and of the frequency of the peak of the corresponding maximum in the rate of change of nonlinear frequency shift (red line) for the rising tone chorus element beginning at $\Omega_e t \sim 2{,}600$ considered in Figure 3. (b) Snapshot at $\Omega_e t = 2{,}875$ of the fluctuation intensity and of the $\partial_t \omega_{\rm res}$ as a function of frequency.

Further to this, and for the sake of completeness, we would like to recall the previous discussion about the formation of subpackets in connection with Figure 8. Recent statistics of 6 years of Van Allen Probes observations provided by Zhang et al. (2020) have shown that the frequency variation inside sufficiently long chorus wave packets is generally finite, in agreement with Vomvoridis et al. (1982) and Omura et al. (2008) and the present theory expression, Equation 45. However, faster frequency variations were found inside very short packets of duration <30 wave periods. Zhang et al. (2020) explained them as due to trapping effects for relatively high amplitudes, or as due to wave superposition for very short packets of moderate amplitudes and duration <10 wave periods. Such statistical results have been qualitatively reproduced by numerical simulations (Nunn et al., 2021); and other previous works have also found some significant wave superposition during observations and simulations of chorus rising tones (Crabtree et al., 2017; Katoh & Omura, 2016; Li et al., 2011).

As a final remark, we would like to emphasize that the present theoretical analysis can also address some elements of the recent work by Tsurutani et al. (2020), based on observations using Van Allen Probe data and emphasizing that each chorus element is made of discrete subelements with constant frequency. Figure 7, in fact, supports that each nonlinear oscillator has a nonlinear frequency shift in the order of a few percent, consistent with observations by Tsurutani et al. (2020). The discrete steps, which are the essential elements of the rising tone chorus element, are instead beyond the description of the present theoretical study since, by definition in Equation D1, we assume the continuous limit to analytically derive the present reduced model for chorus nonlinear dynamics. Within the same theoretical framework, it would be possible to solve the same equations in discretized form, addressing, thus, the situation described by Tsurutani et al. (2020). This, however, is beyond the scope intended for the present work and hopefully will be addressed in the future.

5. Summary

In this work, we have presented a novel and comprehensive theoretical framework of chorus wave excitation, based on field theoretical methods introduced in Zonca et al. (2017) and in earlier works (Chen & Zonca, 2016; Zonca et al., 2015a, 2015b). This theoretical framework allows us to self-consistently evaluate the renormalized phase space response of suprathermal electrons, i.e., the response accounting for self-interactions in the presence of finite amplitude whistler waves.

We have, furthermore, shown that the renormalized distribution function obeys a Dyson-like equation. Since our present aim is to investigate excitation and chirping of chorus waves, we further simplify the Dyson-like equation by taking its velocity space moments and, ultimately, obtain equations for the nonlinear growth rate and frequency shifts of whistler wave packets excited by an anisotropic (bi-Maxwellian) hot electron distribution function. Based on the structure of the hence derived governing equations, we analytically demonstrate for the first time that the chorus chirping rate is given by Equation 1, originally

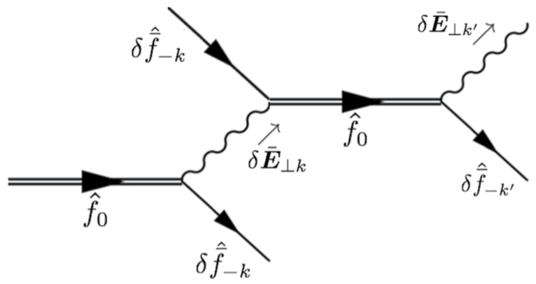

Figure 10. Diagrammatic representation of chorus chirping consistent with the "rules" introduced in Figure B1. The renormalized response of suprathermal electrons, represented by the double solid line propagator, is unstable and emits and reabsorbs same-k fluctuations, which is the strongest nonlinear process on long times. Chorus chirping occurs because, at subsequent times, different k's maximize wave particle power transfer (Zonca et al., 2017).

proposed by Vomvoridis et al. (1982). As argued by Omura et al. (2008) and Vomvoridis et al. (1982), chorus chirping is due to maximization of wave particle power transfer, similar to analogous chirping observed in fusion plasmas (Chen & Zonca, 2016; Zonca et al., 2015a, 2015b). In the light of present results, chorus chirping can be diagrammatically illustrated as in Figure 10. The double solid line propagator represents the renormalized response of suprathermal electrons, which is unstable and, thus, nonlinearly emits oscillators belonging to the whistler spectrum. Emission and reabsorption of the same-k has the strongest cross section (Chen & Zonca, 2016; Zonca et al., 2015a, 2015b). As time progresses, emissions are those that maximize wave particle power transfer and, thus, chirping occurs spontaneously.

The generality of the present theoretical approach goes well beyond the analytic derivation of (Vomvoridis et al., 1982) result of chorus chirping. It provides the insights for reconciling the present interpretation of chorus chirping with that originally provided by Omura and Nunn (2011). It also addresses the physics underlying the evidence of a small nonlinear frequency shift compared with the dynamic range of chorus frequency sweeping, as recently noted by Tsurutani et al. (2020). Meanwhile, it illuminates the origin of chorus subelements being the nonlinear phase modulation analogous to the process introduced by O'Neil (1965).

The present theoretical approach also sheds light on the profound analogies of chorus chirping in space physics and similar nonperturbative frequency sweeping modes in fusion plasmas. In fact, the essential common elements are the narrow fluctuation spectrum of chirping modes that are resonantly excited from a dense background of waves by suprathermal particles, which respond nonperturbatively to maximize wave particle power transfer (Chen & Zonca, 2016; Zonca et al., 2015b).

Last but not least, this theoretical approach provides a direct proof of the one-on-one correspondence of chorus chirping with superradiance in free electron lasers, noted first by Zonca et al. (2015b) and Chen and Zonca (2016). It is also worthwhile emphasizing that the theoretical approaches presented in this work have interesting possible applications to nonlinear phenomena in high power radiation devices such as gyrotron backwave oscillators, where they may not only be applied, but also yield in-depth understandings (Chen & Chen, 2012, 2013).

Appendix A: The Chorus Linear Dispersion Relation

Here, we briefly derive the liner dispersion relation for chorus fluctuations (Kennel & Petschek, 1966), emphasizing the properties that are used for discussing the nonlinear physics addressed in this work. Reconsider Equations 16 and 20, and cast them as follows:

$$\begin{aligned} W(z,t,\omega) + i\Gamma(z,t,\omega) &= \frac{\omega_p^2}{n\omega\partial D_w/\partial\omega}\left\langle \frac{v_\perp^2/2}{\Omega + kv_\parallel - \omega}\left[\frac{k}{\omega}\frac{\partial f_0}{\partial v_\parallel} + \left(1 - \frac{kv_\parallel}{\omega}\right)\frac{1}{v_\perp}\frac{\partial f_0}{\partial v_\perp}\right]\right\rangle \\ &= \frac{\omega(\Omega-\omega)^2}{n\Omega}\left\langle \frac{v_\perp^2/2}{\Omega + kv_\parallel - \omega}\left[\frac{k}{\omega}\frac{\partial f_0}{\partial v_\parallel} - \frac{2}{v_\perp^2}\left(1 - \frac{kv_\parallel}{\omega}\right)f_0\right]\right\rangle, \end{aligned} \tag{A1}$$

where, in the second line, we have integrated by parts in $v_\perp$ and used Equation 6 to make $\partial D_w/\partial\omega$ explicit, assuming $\omega^2/\omega_p^2 \ll 1$ for simplicity (cf. Section 2.2). Using the initial (linear) expression for f_0 given in Equation 21, the spatial dependence of density and thermal speeds are connected with the magnetic field nonuniformity by the condition that f_0 be a function of constants of motion $\mathcal{E} = v^2/2$ and $\mu = v_\perp^2/2B$. The exponent in the bi-Maxwellian is then written as

$$-\frac{\mathcal{E}}{w_\parallel^2} + \frac{\mu B_e}{w_{\perp e}^2}\frac{B}{B_e}\left(\frac{w_{\perp e}^2}{w_\parallel^2} - \frac{w_{\perp e}^2}{w_\perp^2}\right).$$

For this to be constant for arbitrary $\mathcal{E} = v^2/2$ and $\mu = v_\perp^2/2B$, we need to set $w_\parallel = w_{\parallel e}$ and $w_\perp = \zeta w_{\perp e}$, with $\zeta^{-2} = 1 + A(1 - B_e/B) = 1 + A\xi z^2/(1 + \xi z^2)$, as noted below Equation 21. Furthermore, the prefactor in the bi-Maxwellian is constant only if $n_0/n_e = w_\perp^2/w_{\perp e}^2 = \zeta^2$. Meanwhile, performing the velocity space integration, it is possible to write

$$\begin{aligned} W(z,0,\omega) + i\Gamma(z,0,\omega) &= \frac{n_e(\Omega-\omega)^2}{n\Omega}\zeta^2\left[1-(A+1)\zeta^2+(A+1)\zeta^2\frac{(\Omega-\omega)}{\sqrt{2}|k|w_{\parallel e}}Z\left(\frac{\omega-\Omega}{\sqrt{2}|k|w_{\parallel e}}\right)\right. \\ &\left.-\frac{\Omega}{\sqrt{2}|k|w_{\parallel e}}Z\left(\frac{\omega-\Omega}{\sqrt{2}|k|w_{\parallel e}}\right)\right]. \end{aligned} \tag{A2}$$

Here, from Section 2.1, we have recalled $n_0 = \zeta^2 n_e$ and $Z(x) = \pi^{-1/2}\int_{-\infty}^{\infty} e^{-y^2}/(y-x)dy$ is the plasma dispersion function. Noting $A + 1 - \zeta^{-2} = A/(1 + \xi z^2)$, Equation A2 can be rewritten as

$$W(z,0,\omega) + i\Gamma(z,0,\omega) = \frac{n_e(\Omega-\omega)^2}{n\Omega}\zeta^4\left[-\frac{A}{1+\xi z^2}+\frac{A\Omega_e-(A+1)\omega}{\sqrt{2}|k|w_{\parallel e}}Z\left(\frac{\omega-\Omega}{\sqrt{2}|k|w_{\parallel e}}\right)\right]. \tag{A3}$$

This expression shows that $\omega/\Omega_e = A/(A + 1)$ is the frequency where wave particle power exchange with hot electrons changes sign and the driving rate becomes a damping (Kennel & Petschek, 1966). Meanwhile, Equation A3 also shows that $W(z, 0, \omega)$ and $\Gamma(z, 0, \omega)$ scale as ζ^4. Thus, recalling from Section 2.1 that $\zeta^{-2} = 1 + A\xi z^2/(1 + \xi z^2)$, the length scale of the hot electron contribution to the chorus dispersion relation is $\sim(A\xi)^{-1/2}$, which, already at moderate values of A, rapidly takes over the nonuniformity due to the ambient magnetic field, that is $B = B_e(1 + \xi z^2)$ (Helliwell, 1967), as illustrated in Figure 1. This suggests that formal simplification can be achieved in the analytical investigation of chorus nonlinear dynamics, addressed in this work, by assuming a nonuniform source of hot electrons, localized about the equator, neglecting, meanwhile, magnetic field nonuniformity. As noted in Section 2.1, this assumption, although not strictly necessary, helps simplifying the analytical derivations in this work; and can be formally obtained for $A \gg 1$. In fact, as noted above, the $\sim(A\xi)^{-1/2}$ length scale in the hot electron nonuniform response takes over the magnetic field nonuniformity already at moderate values of A.

Appendix B: The Dyson-Schwinger Equation Approach

Here, we elaborate the Dyson-Schwinger equation approach presented in Chen and Zonca (2016) and Zonca et al. (2015b), with the applications to magnetized fusion plasma presented therein, specializing it to nonlinear dynamics and phase space transport by chorus emission.

The "Dyson-like equation" terminology, by analogy with the earlier work by Al'Tshul' and Karpman (1966), was introduced by Chen and Zonca (2016) and Zonca et al. (2015b) as a tribute to Freeman J. Dyson, who recently passed away (https://en.wikipedia.org/wiki/Freeman_Dyson). The Dyson-Schwinger equations, as equations of motion of Green functions, provide a complete description of the theory (Dyson, 1949), since they describe the propagation as well as interaction of the fields themselves. From this point of view, Dyson-Schwinger equations, and Equation 33 as a particular case, can be used to generate perturbation expansions in the weak field limit, cf. Figure B1b, but can also be adopted for the more general strong-coupling case.

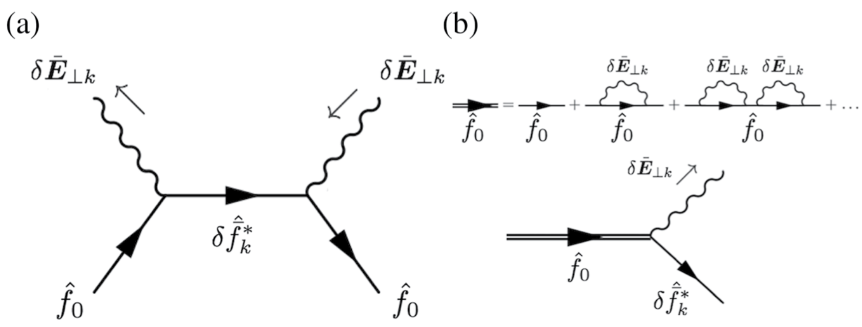

Figure B1. (a) Diagrammatic representation of the elementary processes of Equations 32 and 33. (b) Diagrammatic representation of the renormalized $\hat{f}_0$ hot electron response as solution of the Dyson-like Equation 33.

The elementary process that underlies this dynamics is illustrated in Figure B1a, where we have borrowed and suitably modified the Feynman diagram rules as in Chen and Zonca (2016) and Zonca et al. (2017) to illustrate Equation 32 and its reverse. In particular, straight lines represent linearized propagators (Green functions) of particle distribution functions, while wavy lines stand for linearized propagators (Green functions) of fluctuating electromagnetic fields. Arrows indicate the direction of propagation. Meanwhile, nodes represent (nonlinear) interactions/couplings. Furthermore, because of energy and momentum conservation in particle and electromagnetic fields field interactions, propagation of fields is equivalent to the opposite propagation of corresponding complex conjugate fields (Zonca et al., 2015a). For example, emission of $\delta \bar{E}_k$ corresponds to absorption of $\delta \bar{E}_k^*$ because of symmetry under parity and time reversal transformations. Thus, the left node (vertex) in Figure B1a represents (the *c.c.* of) Equation 32; while the right node (vertex) represents the first two lines of Equation 33. In the present theoretical approach, emission and reabsorption of $\delta \bar{E}_k$ and $\delta \bar{E}_k^*$ can occur repeatedly. Here, by emission we mean "generation of waves" because of the instability driven by the spatially averaged electron distribution function $\hat{f}_0$. Meanwhile, by reabsorption we intend to mean the "nonlinear interaction" of electromagnetic fluctuations with the perturbed electron distribution function that modifies $\hat{f}_0$ itself. This is illustrated in the upper part of Figure B1b in the form of a Dyson series, and dominates the nonlinear dynamics since it can be shown to cause the most significant distortion of $\hat{f}_0$ on the long time scale (Aamodt, 1967; Al'Tshul & Karpman, 1966; Balescu, 1963; Chen & Zonca, 2016; Dupree, 1966; Mima, 1973; Prigogine, 1962; van Hove, 1954; Weinstock, 1969; Zonca et al., 2015a, 2015b, 2017). Such a distortion of the hot electron distribution function, determined self-consistently in the presence of the finite amplitude fluctuation spectrum, constitutes the "renormalized" hot electron response, denoted with the double solid line in Figure B1b. It is this renormalized hot electron $\hat{f}_0$, which is evolving in time, that self-consistently causes the evolution of the fluctuation spectrum according to Equations 11–16 and as illustrated in the lower part of Figure B1b. Equation 33, meanwhile, is a nonlinear integro-differential equation and can be used to close the chorus wave equations discussed in Section 2.1. In fact, it describes the response of the $k = 0$ hot electron distribution function by continuous emission and reabsorption of whistler waves, shown in Figure B1b, which are amplified due to wave particle resonant interactions. Again, we note that this emission and reabsorption occur with any generic whistler wave packet as denoted by the summation over the whole fluctuation spectrum, which is evolving in time self-consistently with the $k = 0$ particle distribution function. In this respect, as noted already, Equation 33 can be viewed as the renormalized hot electron distribution function evolving on the nonlinear time scale, which justifies dubbing it as Dyson-like equation (Chen & Zonca, 2016; Zonca et al., 2015a, 2015b).

Appendix C: Detailed Derivation of Equations 37 and 38

C1. Derivation of Equation 37

In this appendix, we briefly summarize the derivation of Equation 37 from Equation 27 based on Equations 33 and 36. For consistency with Section 3, we also denote the current frequency and wave number satisfying the lowest order whistler wave dispersion relation as $\bar{\omega}$ and $\bar{k}$ in order to distinguish them from ω and k in the running summation over the fluctuation spectrum. Formally, we can rewrite Equation 27 as

$$\begin{aligned} \bar{W}(\bar{\omega}) + i\bar{\Gamma}(\bar{\omega}) \quad &= \quad \frac{n_e}{n}\left(1 - \frac{v_{r\bar{\omega}}}{v_{g\bar{\omega}}}\right)^2 \left\langle \frac{v_\perp^2}{2}\Omega_e\left[\Omega_e + \bar{k}v_\parallel - \bar{\omega} - i(1 - v_{r\bar{\omega}}/v_{g\bar{\omega}})\partial_t\right]^{-1} \right. \\ &\quad \left. \times \left(\frac{\bar{k}}{\bar{\omega}}\frac{\partial}{\partial v_\parallel} - \frac{2}{v_\perp^2}\frac{\Omega_e}{\bar{\omega}}\right)(\partial_t + v_\parallel\partial_z)^{-1}(\partial_t + v_\parallel\partial_z)\,\hat{f}_0 \right\rangle, \end{aligned} \tag{C1}$$

where, for brevity, we have omitted the dependences on $t - z/v_{g\bar{\omega}}$. From this, upon substitution of Equation 33 and noting Equation 36, we have

$$
\begin{aligned}
\bar{W}(\bar{\omega}) + i\bar{\Gamma}(\bar{\omega}) &= \frac{n_e}{n}\left(1-\frac{v_{r\bar{\omega}}}{v_{g\bar{\omega}}}\right)^2 \left\langle \frac{v_\perp^2}{2}\Omega_e\left[\Omega_e + \bar{k}v_\parallel - \bar{\omega} - i(1-v_{r\bar{\omega}}/v_{g\bar{\omega}})\partial_t\right]^{-1} \right.\\
&\times\left(\frac{\bar{k}}{\bar{\omega}}\frac{\partial}{\partial v_\parallel} - \frac{2}{v_\perp^2}\frac{\Omega_e}{\bar{\omega}}\right)\sum_k \frac{e^2}{2m^2}v_\perp|\delta\bar{E}_k|\left[\frac{k}{\omega}\frac{\partial}{\partial v_\parallel} + \left(1-\frac{kv_\parallel}{\omega}\right)\left(\frac{1}{v_\perp}\frac{\partial}{\partial v_\perp}+\frac{1}{v_\perp^2}\right)\right]\\
&\times\left[(\Omega_e + kv_\parallel - \omega)^2 + (1-v_{r\omega}/v_{g\omega})^2\partial_t^2\right]^{-1}(1-v_{r\omega}/v_{g\omega})\partial_t v_\perp|\delta\bar{E}_k|\\
&\left.\times\left[\frac{k}{\omega}\frac{\partial}{\partial v_\parallel} + \left(1-\frac{kv_\parallel}{\omega}\right)\frac{1}{v_\perp}\frac{\partial}{\partial v_\perp}\right]\hat{f}_0\right\rangle\\
&\simeq \frac{n_e}{n}\left(1-\frac{v_{r\bar{\omega}}}{v_{g\bar{\omega}}}\right)^2 \left\langle \frac{v_\perp^2}{2}\Omega_e\left[\Omega_e + \bar{k}v_\parallel - \bar{\omega} - i(1-v_{r\bar{\omega}}/v_{g\bar{\omega}})\partial_t\right]^{-1} \right.\\
&\times\left(\frac{\bar{k}}{\bar{\omega}}\frac{\partial}{\partial v_\parallel} - \frac{2}{v_\perp^2}\frac{\Omega_e}{\bar{\omega}}\right)\sum_k \frac{e^2}{2m^2}v_\perp|\delta\bar{E}_k|\left[\frac{k}{\omega}\frac{\partial}{\partial v_\parallel} + \frac{\Omega_e}{\omega}\left(\frac{1}{v_\perp}\frac{\partial}{\partial v_\perp}+\frac{1}{v_\perp^2}\right)\right]\\
&\times\left[(\Omega_e + kv_\parallel - \omega)^2 + (1-v_{r\omega}/v_{g\omega})^2\partial_t^2\right]^{-1}(1-v_{r\omega}/v_{g\omega})\partial_t v_\perp|\delta\bar{E}_k|\\
&\left.\times\left[\frac{k}{\omega}\frac{\partial}{\partial v_\parallel} + \frac{\Omega_e}{\omega}\frac{1}{v_\perp}\frac{\partial}{\partial v_\perp}\right]\hat{f}_0\right\rangle.
\end{aligned}
\tag{C2}
$$

To derive Equation 37, the last step is to integrate by parts twice in $v_\perp$ in order to eliminate $\partial_{v_\perp}$, taking into account that

$$
\left\langle v_\perp^4 \hat{f}_0\right\rangle = 2\frac{\left\langle v_\perp^2\hat{f}_0\right\rangle^2}{\left\langle \hat{f}_0\right\rangle}, \tag{C3}
$$

for the anisotropic Maxwellian of Equation 21.

C2. Derivation of Equation 38

Velocity space integration in Equation 37 is naturally (and more rigorously) performed in the Laplace-rather than in the time-representation (Chen & Zonca, 2016; Tao et al., 2020; Zonca et al., 2015b, 2017). Here, however, for the sake of simplicity and conciseness, we directly manipulate Equation 37 in the time-representation formally handling operator symbols. Let us first note, considering Equation 35

$$
\begin{aligned}
\left[\Omega_e + \bar{k}v_\parallel - \bar{\omega} - i(1-v_{r\bar{\omega}}/v_{g\bar{\omega}})\partial_t\right]^{-1} &\simeq \left[(\Omega_e + \bar{k}v_\parallel - \bar{\omega})^2 + (1-v_{r\bar{\omega}}/v_{g\bar{\omega}})^2\partial_t^2\right]^{-1}\\
&\quad\times\left[\Omega_e + \bar{k}v_\parallel - \bar{\omega} + i(1-v_{r\bar{\omega}}/v_{g\bar{\omega}})\partial_t\right]\\
&\simeq \left[x^2+a^2\right]^{-1}\left[x+ia\right],
\end{aligned}
\tag{C4}
$$

having denoted symbolically $x \equiv \bar{k}(v_\parallel - v_{r\bar{\omega}})$ and $a \equiv (1-v_{r\bar{\omega}}/v_{g\bar{\omega}})\partial_t$. Here, a as an operator is meant to be acting on $|\delta\bar{E}_{\bar{k}}|$ and what follows in the representation of the integrand, that is $|\delta\bar{E}_k|^2$ and $\hat{f}_0$. In fact, in the derivation of Equations 20 and 25, we have normalized the wave particle power exchange to $|\delta\bar{E}_{\bar{k}}|^2$. Thus, the nonlinear frequency and wave number shift due to the incremental change in the wave packet amplitude and phase are reabsorbed into $\bar{k}(v_\parallel - v_{r\bar{\omega}})$ as will be further discussed in Section 4. We can adopt the same symbolic representation for Equation 36 and, thus

$$
\left[(\Omega_e + kv_\parallel - \omega)^2 + (1-v_{r\omega}/v_{g\omega})^2\partial_t^2\right]^{-1}(1-v_{r\omega}/v_{g\omega})\partial_t \simeq \left[(x-x_0)^2+b^2\right]^{-1}b, \tag{C5}
$$

where $x_0 \equiv \omega - \bar{\omega} - v_{r\omega}(k-\bar{k}) \simeq (1-v_{r\omega}/v_{g\omega})(\omega-\bar{\omega})$ and $b \equiv (1-v_{r\omega}/v_{g\omega})\partial_t$ as an operator is meant to be acting on $|\delta\bar{E}_k|$ and $\hat{f}_0$. Meanwhile, for resonant particles, we note that, for $\mathbb{R}ea > 0$, $\mathbb{R}eb > 0$ and $|a|, |b|, |x_0| \ll 1$

$$\left[x^2+a^2\right]^{-1}a\left[(x-x_0)^2+b^2\right]^{-1}b \simeq (\pi/2)\left[x_0^2+(a+b)^2\right]^{-1}(a+b)\left(\delta(x)+\delta(x-x_0)\right) -(\pi/2)\left[x_0^2+(a-b)^2\right]^{-1}(a-b)\left(\delta(x)-\delta(x-x_0)\right), \tag{C6}$$

inside the velocity space integrand; and

$$\left[x^2+a^2\right]^{-1}x\left[(x-x_0)^2+b^2\right]^{-1}b \simeq (\pi/2)\left[x_0^2+(a+b)^2\right]^{-1}x_0\left(\delta(x)+\delta(x-x_0)\right) -(\pi/2)\left[x_0^2+(a-b)^2\right]^{-1}x_0\left(\delta(x)-\delta(x-x_0)\right). \tag{C7}$$

Terms depending on $\delta(x)$ in the velocity space integrand are computed at $v_\parallel = v_{r\omega}$, while those depending on $\delta(x-x_0)$ are computed at $v_\parallel = v_{r\bar{\omega}}$. We can further simplify these expressions noting that, for a narrow spectrum, contributions $\propto (\delta(x)-\delta(x-x_0))$ can be neglected. Furthermore, the symbolic expression of $(a+b)$ can also be simplified noting assumption (a) in Section 3 and, thus

$$\begin{aligned}(a+b) &\simeq |\delta\bar{E}_k|^{-3}\hat{f}_0^{-1}(1-v_{r\omega}/v_{g\omega})\partial_t|\delta\bar{E}_k|^3\hat{f}_0 \\ &\quad +|\delta\bar{E}_k|^{-1}\hat{f}_0^{-1}(1-v_{r\omega}/v_{g\omega})\partial_t|\delta\bar{E}_k|\hat{f}_0 \\ &\simeq 2|\delta\bar{E}_k|^{-2}\hat{f}_0^{-1}(1-v_{r\omega}/v_{g\omega})\partial_t|\delta\bar{E}_k|^2\hat{f}_0.\end{aligned} \tag{C8}$$

Again, these symbolic relations are more rigorously interpreted in the Laplace-rather than the time-representation (Chen & Zonca, 2016; Tao et al., 2020; Zonca et al., 2015b, 2017). Interested readers are referred to the original references for more details.

Based on these relations, one can derive Equations 38 and 39, where we have noted that

$$\frac{1}{k}\frac{\partial}{\partial v_{r\omega}} = \frac{1}{(1-v_{r\omega}/v_{g\omega})}\frac{\partial}{\partial\omega}, \tag{C9}$$

justifying the usefulness of introducing the normalization of $\bar{W}$ and $\bar{\Gamma}$ as in Equation 27 in Section 2.2. The presence of the integral operator

$$\left[\frac{(\omega-\bar{\omega})^2}{4\Omega_e^2}+\Omega_e^{-2}\partial_t^2\right]^{-1} \tag{C10}$$

is what allows us to neglect the nonresonant particle response (Cauchy principal value) in the derivations above.

Appendix D: Evolution Equations for Numerical Solution of the Reduced Dyson-Like Equation

To exploit the dense nature of the whistler wave spectrum, we introduce the dimensionless intensity $\mathcal{I}(\omega)$ such that

$$\sum_k \frac{\left\langle\left\langle\omega_{\mathrm{trk}}^4\right\rangle\right\rangle}{\Omega_e^4} = \frac{\hat{\gamma}_e^2}{\Omega_e^2}\int\frac{d\omega}{\Omega_e}\mathcal{I}(\omega)\frac{\omega^{3/2}}{(\Omega_e-\omega)^{3/2}}. \tag{D1}$$

Here, the $\omega^{3/2}/(\Omega_e-\omega)^{3/2}$ factor accounts for the $\sim I_k k^3$ scaling of $\left\langle\left\langle\omega_{\mathrm{trk}}^4\right\rangle\right\rangle$. This normalization is chosen ad hoc to have nonlinearity effects being important when $\mathcal{I}(\omega)\sim\mathcal{O}(1)$.

To invert the integral operator of Equation C10, let us introduce the auxiliary functions

$$
\begin{aligned}
\left[\frac{(\omega-\bar{\omega})^2}{4\Omega_e^2}+\Omega_e^{-2}\partial_t^2\right]G_{L1}(\omega,\bar{\omega}) &= \frac{\hat{\gamma}_e^2}{\Omega_e^2}\frac{\mathcal{I}(\omega)}{(1-v_{r\omega}/v_{g\omega})^4}\bar{\Gamma}_L(\omega),\\
\left[\frac{(\omega-\bar{\omega})^2}{4\Omega_e^2}+\Omega_e^{-2}\partial_t^2\right]G_{L2}(\omega,\bar{\omega}) &= \frac{\hat{\gamma}_e^2}{\Omega_e^2}\frac{\mathcal{I}(\omega)}{(1-v_{r\omega}/v_{g\omega})^4}\bar{\Gamma}_L(\bar{\omega}),\\
\left[\frac{(\omega-\bar{\omega})^2}{4\Omega_e^2}+\Omega_e^{-2}\partial_t^2\right]G_{NL1}(\omega,\bar{\omega}) &= \frac{\hat{\gamma}_e^2}{\Omega_e^2}\frac{\mathcal{I}(\omega)}{(1-v_{r\omega}/v_{g\omega})^4}\bar{\Gamma}_{NL}(\omega),\\
\left[\frac{(\omega-\bar{\omega})^2}{4\Omega_e^2}+\Omega_e^{-2}\partial_t^2\right]G_{NL2}(\omega,\bar{\omega}) &= \frac{\hat{\gamma}_e^2}{\Omega_e^2}\frac{\mathcal{I}(\omega)}{(1-v_{r\omega}/v_{g\omega})^4}\bar{\Gamma}_{NL}(\bar{\omega});
\end{aligned}
\tag{D2}
$$

where, from Equation 39

$$
\begin{aligned}
\bar{\Gamma}_{NL}(\bar{\omega}) \;=\; & \left[\Omega_e\frac{\partial}{\partial\bar{\omega}}-\frac{2\Omega_e^2}{\bar{k}^2\left\langle v_\perp^2\right\rangle}\left(1-\frac{v_{r\bar{\omega}}}{v_{g\bar{\omega}}}\right)\right]\Omega_e\frac{\partial}{\partial\bar{\omega}}\int\frac{d\omega}{\Omega_e}\frac{\omega^{3/2}}{(\Omega_e-\omega)^{3/2}}\\
&\times\frac{1}{8}\left[G_{L1}(\omega,\bar{\omega})+G_{L2}(\omega,\bar{\omega})+G_{NL1}(\omega,\bar{\omega})+G_{NL2}(\omega,\bar{\omega})\right].
\end{aligned}
\tag{D3}
$$

Meanwhile, Equation 38 can be cast as

$$
\begin{aligned}
\Omega_e^{-1}\partial_t\bar{W}(\bar{\omega}) \;=\; & \left[\Omega_e\frac{\partial}{\partial\bar{\omega}}-\frac{2\Omega_e^2}{\bar{k}^2\left\langle v_\perp^2\right\rangle}\left(1-\frac{v_{r\bar{\omega}}}{v_{g\bar{\omega}}}\right)\right]\Omega_e\frac{\partial}{\partial\bar{\omega}}\int\frac{d\omega}{\Omega_e}\frac{\omega^{3/2}}{(\Omega_e-\omega)^{3/2}}\frac{(\omega-\bar{\omega})}{2\Omega_e}\\
&\times\frac{1}{8}\left[G_{L1}(\omega,\bar{\omega})+G_{L2}(\omega,\bar{\omega})+G_{NL1}(\omega,\bar{\omega})+G_{NL2}(\omega,\bar{\omega})\right].
\end{aligned}
\tag{D4}
$$

Equations D2–D4 are closed by the intensity evolution equation,

$$
\begin{aligned}
\Omega_e^{-1}\partial_t\mathcal{I}(\omega) \;=\; & 2\mathcal{S}\mathcal{I}(\omega)^{1/2}+2\mathcal{I}(\omega)\frac{\omega(\Omega_e-\omega)^2}{\Omega_e^3}\left[\partial_t\left(\int_{z-v_{g\omega}t}^{\infty}\zeta^4(z')\frac{dz'}{v_{g\omega}}\right)\bar{\Gamma}(\omega)\right.\\
&\left.+\left(\int_{z-v_{g\omega}t}^{\infty}\zeta^4(z')\frac{dz'}{v_{g\omega}}\right)\partial_t\bar{\Gamma}(\omega)\right]\Big/\left(1-\frac{v_{r\omega}}{v_{g\omega}}\right)^2;
\end{aligned}
\tag{D5}
$$

and the wave packet phase evolution equation

$$
\begin{aligned}
\Omega_e^{-1}\partial_t\varphi(\omega) \;=\; & -\frac{\omega(\Omega_e-\omega)^2}{\Omega_e^3}\left[\partial_t\left(\int_{z-v_{g\omega}t}^{\infty}\zeta^4(z')\frac{dz'}{v_{g\omega}}\right)\bar{W}(\omega)\right.\\
&\left.+\left(\int_{z-v_{g\omega}t}^{\infty}\zeta^4(z')\frac{dz'}{v_{g\omega}}\right)\partial_t\bar{W}(\omega)\right]\Big/\left(1-\frac{v_{r\omega}}{v_{g\omega}}\right)^2;
\end{aligned}
\tag{D6}
$$

which can be readily derived from Equations 11 and 14 keeping in mind the discussion given in the first paragraph of Section 3. Note that we have added a source term $2\mathcal{S}\mathcal{I}(\omega)^{1/2}$ on the right-hand side of Equation D5. The value of $\mathcal{S}$ represents the injection rate of fluctuations in the $|\delta\bar{E}_k|$ spectrum. We adopted it because it gives us a variety of possibilities rather than assuming an initial spectrum; e.g., using $\mathcal{S}$ as a random source stirring the system or a constant uniform source. Figure D1 gives a comparison of the linear evolution of $\mathcal{I}(z=50c/\omega_e,t,\omega)$ in the case of a random (a) and uniform source (b) of the same strength $\mathcal{S}=2\times10^{-5}$. Parameters are the same as in Figure 1. In both cases, we clearly note the predominance of a narrow spectrum at the most unstable frequency after the whistler wave packet has been convectively amplified by crossing the localized hot electron source at the equator. Because of this, we will focus on the uniform source case in the following, and discuss random or more general sources in later studies. Equations D2–D6 fully characterize the self-consistent nonlinear evolution of a whistler wave packet spectrum excited by wave particle resonances with a hot electron source that is localized about the equator. As anticipated in Sections 2.2 and 3, they assume that the whistler wave packets belong to a dense (nearly continuous) spectrum that are continuously emitted and reabsorbed (cf. Figure B1 and corresponding discussion) to maximize wave particle power transfer (Chen & Zonca, 2016; Zonca et al., 2015b). When solving these equations by advancing them in time by one step Δt, one has to keep in mind that the wave packet amplitude and phase are shifted nonlinearly and cause hot electron induced frequency ($\Delta(\Delta_\omega)=-\Delta t\partial_t^2\varphi(\omega)$) and corresponding wave number shifts, introduced in Section 2.2. Despite $\Delta_\omega/\Delta_k=v_{g\omega}$, and, thus, the shifted wave packet still satisfies the whistler dispersion relation, the hot electron induced phase shift causes a corresponding

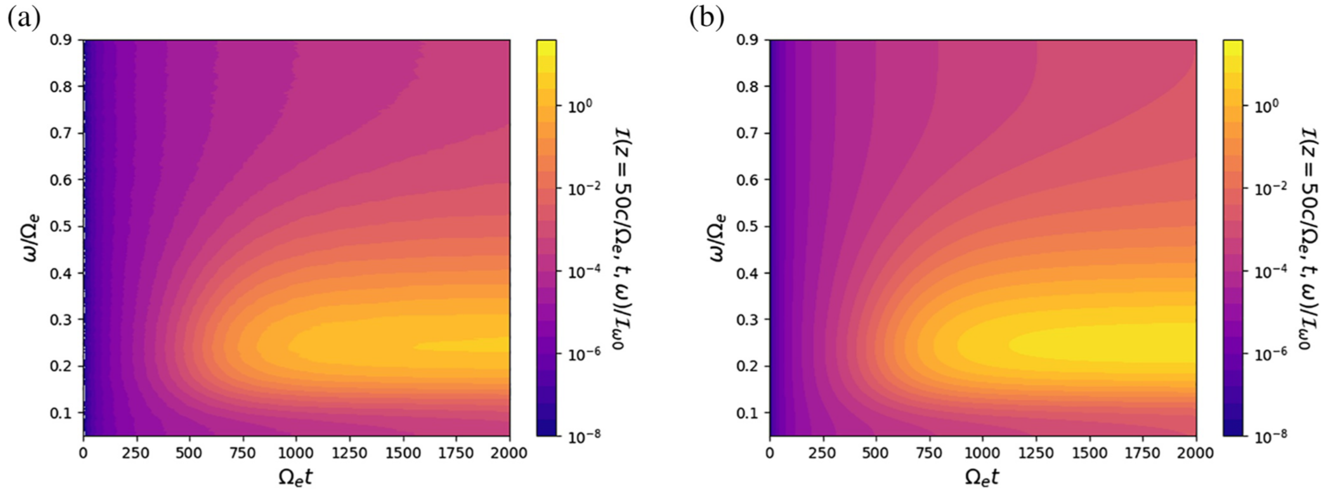

Figure D1. Contour plot of the linear evolution of $\mathcal{I}(z = 50c/\omega_e, t, \omega)$ for (a) a random source and (b) a uniform source of the same strength $\mathcal{S} = 2 \times 10^{-5}$ in Equation D5. The position is fixed at $z\Omega_e/c = 50$ and parameters are the same as in Figure 1.

small but finite shift in the resonant velocity $k\Delta v_{r\omega} = \Delta_\omega - v_{r\omega}\Delta_k = (1 - v_{r\omega}/v_{g\omega})\Delta_\omega$. This means that, after advancing in time by one step Δt, the functions $\bar{\Gamma}_{NL}$ and $\bar{W}_{NL}$ are actually evaluated at $\bar{\omega} + \Delta(\Delta_\omega)$. Thus, noting Equation C9, these functions have to be updated as

$$\begin{aligned} \bar{\Gamma}_{NL}(\bar{\omega}) &\rightarrow \bar{\Gamma}_{NL}(\bar{\omega}) - \Delta(\Delta_\omega)\frac{\partial}{\partial\bar{\omega}}\bar{\Gamma}_{NL}(\bar{\omega}), \\ \bar{W}_{NL}(\bar{\omega}) &\rightarrow \bar{W}_{NL}(\bar{\omega}) - \Delta(\Delta_\omega)\frac{\partial}{\partial\bar{\omega}}\bar{W}_{NL}(\bar{\omega}). \end{aligned} \tag{D7}$$

A similar argument applies to $\mathcal{I}(\omega)$ and $\varphi(\omega)$, such that

$$\begin{aligned} \mathcal{I}(\omega) &\rightarrow \mathcal{I}(\omega) - \Delta(\Delta_\omega)\frac{\partial}{\partial\omega}\mathcal{I}(\omega), \\ \varphi(\omega) &\rightarrow \varphi(\omega) - \Delta(\Delta_\omega)\frac{\partial}{\partial\omega}\varphi(\omega); \end{aligned} \tag{D8}$$

after each time step. Note that Equation D8 corresponds to changing $\partial_t \rightarrow \partial_t - \partial_t^2\varphi(\omega)\partial_\omega$ on the left-hand side of Equations D5 and D6; i.e., to solving the wave kinetic equation (Bernstein & Baldwin, 1977; McDonald, 1988) for wave packet intensity and phase.

Considering $\mathcal{I}(\omega) = 0$ together with $\varphi(\omega) = 0$ at $t = 0$, initial conditions for Equation D2 are particularly simple

$$\begin{aligned} G_{\dots}(\omega, \bar{\omega})|_{t=0} &= 0, \\ \partial_t G_{\dots}(\omega, \bar{\omega})|_{t=0} &= 0, \end{aligned} \tag{D9}$$

where, for brevity, we have generically denoted by … the subscripts of $G_{\dots}(\omega, \bar{\omega})$ functions defined in Equation D2. Furthermore, for Equations D3 and D4

$$\begin{aligned} \bar{\Gamma}_{NL}(\omega)|_{t=0} &= 0, \\ \bar{W}_{NL}(\omega)|_{t=0} &= 0. \end{aligned} \tag{D10}$$

Finally, considering a frequency domain such that the fluctuation spectrum at the boundary is sufficiently small that it can be neglected, boundary conditions are the trivial ones; i.e., $G_{\dots}(\omega, \bar{\omega})$ functions, $\bar{\Gamma}_{NL}(\omega)$ and $\bar{W}_{NL}(\omega)$ vanish at any time. However, more realistically and to avoid undesirable discontinuities at the boundary of the frequency simulation domain, we assume that values at the boundaries are obtained by linear extrapolation of the inner solution.

Data Availability Statement

Code and input files used for generating the data used in this study can be found at https://doi.org/10.5281/zenodo.5076015.

Acknowledgments
This work was carried out within the framework of the EUROfusion Consortium and received funding from Euratom research and training programme 2014–2018 and 2019–2020 under Grant Agreement No. 633053 (Project No. WP19-ER/ENEA-05). The views and opinions expressed herein do not necessarily reflect those of the European Commission. This work was also supported by the NSFC Grants (42174182 and 11235009), the Strategic Priority Program of the Chinese Academy of Sciences (No. XDB41000000), and the Fundamental Research Funds for the Central Universities. Open Access Funding provided by ENEA Agenzia Nazionale per Le Nuove Tecnologie l'Energia e lo Sviluppo Economico Sostenibile within the CRUI-CARE Agreement.

References

Aamodt, R. E. (1967). Test waves in weakly turbulent plasmas. *The Physics of Fluids*, *10*(6), 1245–1250. https://doi.org/10.1063/1.1762269
Al'Tshul', L. M., & Karpman, V. I. (1966). Theory of nonlinear oscillations in a collisionless plasma. *Journal of Experimental and Theoretical Physics*, *22*, 361–369.
Balescu, R. (1963). *Statistical mechanics of charged particles*. New York, NY: Interscience.
Bernstein, I. B., & Baldwin, D. E. (1977). Geometric optics in space and time varying plasmas. II. *The Physics of Fluids*, *20*(1), 116–126. https://doi.org/10.1063/1.861700
Bortnik, J., & Thorne, R. (2007). The dual role of ELF/VLF chorus waves in the acceleration and precipitation of radiation belt electrons. *Journal of Atmospheric and Solar-Terrestrial Physics*, *69*, 378–386. https://doi.org/10.1016/j.jastp.2006.05.030
Burtis, W. J., & Helliwell, R. A. (1976). Magnetospheric chorus: Occurrence patterns and normalized frequency. *Planetary and Space Science*, *24*(11), 1007–1010. https://doi.org/10.1016/0032-0633(76)90119-7
Chen, L., & Zonca, F. (2016). Physics of Alfvén waves and energetic particles in burning plasmas. *Reviews of Modern Physics*, *88*, 015008. https://doi.org/10.1103/RevModPhys.88.015008
Chen, S.-H., & Chen, L. (2012). Linear and nonlinear behaviors of gyrotron backward wave oscillators. *Physics of Plasmas*, *19*, 023116. https://doi.org/10.1063/1.3688892
Chen, S.-H., & Chen, L. (2013). Nonstationary oscillation of gyrotron backward wave oscillators with cylindrical interaction structure. *Physics of Plasmas*, *20*, 123108. https://doi.org/10.1063/1.4846876
Chen, Y., Reeves, G. D., & Friedel, R. H. W. (2007). The energization of relativistic electrons in the outer Van Allen radiation belt. *Nature Physics*, *3*, 614–617. https://doi.org/10.1038/nphys655
Crabtree, C., Tejero, E., Ganguli, G., Hospodarsky, G. B., & Kletzing, C. A. (2017). Bayesian spectral analysis of chorus subelements from the Van Allen Probes. *Journal of Geophysical Research: Space Physics*, *122*, 6088–6106. https://doi.org/10.1002/2016JA023547
Cully, C. M., Angelopoulos, V., Auster, U., Bonnell, J., & Le Contel, O. (2011). Observational evidence of the generation mechanism for rising-tone chorus. *Geophysical Research Letters*, *38*, L01106. https://doi.org/10.1029/2010GL045793
Demekhov, A. (2011). Generation of VLF emissions with the increasing and decreasing frequency in the magnetospheric cyclotron maser in the backward wave oscillator regime. *Radiophysics and Quantum Electronics*, *53*, 609. https://doi.org/10.1007/s11141-011-9256-x
Dupree, T. H. (1966). A perturbation theory for strong plasma turbulence. *Physics of Fluids*, *9*(9), 1773–1782. https://doi.org/10.1063/1.1761933
Dyson, F. J. (1949). The *s* matrix in quantum electrodynamics. *Physical Review*, *75*, 1736–1755. https://doi.org/10.1103/PhysRev.75.1736
Hanzelka, M., Santolík, O., Omura, Y., Kolmasová, I., & Kletzing, C. A. (2020). A model of the subpacket structure of rising tone chorus emissions. *Journal of Geophysical Research: Space Physics*, *125*, e2020JA028094. https://doi.org/10.1029/2020JA028094
Helliwell, R. A. (1967). A theory of discrete VLF emissions from the magnetosphere. *Journal of Geophysical Research*, *72*(19), 4773–4790.
Hikishima, M., & Omura, Y. (2012). Particle simulations of whistler-mode rising-tone emissions triggered by waves with different amplitudes. *Journal of Geophysical Research*, *117*, A04226. https://doi.org/10.1029/2011JA017428
Horne, R. B., & Thorne, R. M. (1998). Potential waves for relativistic electron scattering and stochastic acceleration during magnetic storms. *Geophysical Research Letters*, *25*(15), 3011–3014.
Horne, R. B., Thorne, R. M., Shprits, Y. Y., Meredith, N. P., Glauert, S. A., Smith, A. J., & Decreau, P. M. E. (2005). Wave acceleration of electrons in the Van Allen radiation belts. *Nature*, *437*, 227–230. https://doi.org/10.1038/nature03939
Itzykson, C., & Zuber, J.-B. (1980). *Quantum field theory*. New York, NY: McGraw-Hill.
Katoh, Y., & Omura, Y. (2011). Amplitude dependence of frequency sweep rates of whistler mode chorus emissions. *Journal of Geophysical Research*, *116*, A07201. https://doi.org/10.1029/2011JA016496
Katoh, Y., & Omura, Y. (2013). Effect of the background magnetic field inhomogeneity on generation processes of whistler-mode chorus and broadband hiss-like emissions. *Journal of Geophysical Research: Atmospheres*, *118*, 4189–4198. https://doi.org/10.1002/jgra.50395
Katoh, Y., & Omura, Y. (2016). Electron hybrid code simulation of whistler-mode chorus generation with real parameters in the Earth's inner magnetosphere. *Earth Planets and Space*, *68*, 192. https://doi.org/10.1186/s40623-016-0568-0
Kennel, C. F., & Petschek, H. E. (1966). Limit on stably trapped particle fluxes. *Journal of Geophysical Research*, *71*(1), 1–28.
Li, W., Thorne, R. M., Bortnik, J., Shprits, Y. Y., Nishimura, Y., Angelopoulos, V., & Bonnell, J. W. (2011). Typical properties of rising and falling tone chorus waves. *Geophysical Research Letters*, *38*, L14103. https://doi.org/10.1029/2011GL047925
Macúšová, E., Santolík, O., Décréau, P., Demekhov, A. G., Nunn, D., Gurnett, D. A., & Trotignon, J.-G. (2010). Observations of the relationship between frequency sweep rates of chorus wave packets and plasma density. *Journal of Geophysical Research*, *115*, A12257. https://doi.org/10.1029/2010JA015468
McDonald, S. W. (1988). Phase-space representations of wave equations with applications to the eikonal approximation for short-wavelength waves. *Physics Reports*, *158*(6), 337–416. https://doi.org/10.1016/0370-1573(88)90012-9
Mima, K. (1973). Modification of weak turbulence theory due to perturbed orbit effects. I. general formulation. *Journal of the Physical Society of Japan*, *34*(6), 1620–1632.
Miyoshi, Y., Katoh, Y., Nishiyama, T., Sakanoi, T., Asamura, K., & Hirahara, M. (2010). Time of flight analysis of pulsating aurora electrons, considering wave-particle interactions with propagating whistler mode waves. *Journal of Geophysical Research*, *115*, A10312. https://doi.org/10.1029/2009JA015127
Mourenas, D., Artemyev, A. V., Agapitov, O. V., Krasnoselskikh, V., & Mozer, F. S. (2015). Very oblique whistler generation by low-energy electron streams. *Journal of Geophysical Research: Space Physics*, *120*, 3665–3683. https://doi.org/10.1002/2015JA021135
Nishimura, Y., Bortnik, J., Li, W., Thorne, R. M., Lyons, L. R., Angelopoulos, V., & Auster, U. (2010). Identifying the driver of pulsating aurora. *Science*, *330*(6000), 81–84. https://doi.org/10.1126/science.1193130
Nunn, D. (1974). A self-consistent theory of triggered VLF emissions. *Planetary and Space Science*, *22*(3), 349–378. https://doi.org/10.1016/0032-0633(74)90070-1
Nunn, D., Zhang, X.-J., Mourenas, D., & Artemyev, A. V. (2021). Generation of realistic short chorus wave packets. *Geophysical Research Letters*, *48*, e2020GL092178. https://doi.org/10.1029/2020GL092178

Omura, Y., Katoh, Y., & Summers, D. (2008). Theory and simulation of the generation of whistler-mode chorus. *Journal of Geophysical Research*, *113*, A04223. https://doi.org/10.1029/2007JA012622

Omura, Y., & Matsumoto, H. (1982). Computer simulations of basic processes of coherent whistler wave-particle interactions in the magnetosphere. *Journal of Geophysical Research*, *87*(A6), 4435–4444. https://doi.org/10.1029/JA087iA06p04435

Omura, Y., & Nunn, D. (2011). Triggering process of whistler mode chorus emissions in the magnetosphere. *Journal of Geophysical Research*, *116*, A05205. https://doi.org/10.1029/2010JA016280

O'Neil, T. (1965). Collisionless damping of nonlinear plasma oscillations. *Physics of Fluids*, *8*, 2255–2262. https://doi.org/10.1063/1.1761193

Prigogine, I. (1962). *Nonequilibrium statistical mechanics*. New York, NY: Interscience.

Reeves, G. D., Spence, H. E., Henderson, M. G., Morley, S. K., Friedel, R. H. W., Funsten, H. O., & Niehof, J. T. (2013). Electron acceleration in the heart of the Van Allen radiation belts. *Science*, *341*(6149), 991–994. https://doi.org/10.1126/science.1237743

Santolík, O., Gurnett, D. A., Pickett, J. S., Parrot, M., & Cornilleau-Wehrlin, N. (2003). Spatio-temporal structure of storm-time chorus. *Journal of Geophysical Research*, *108*(A7), 1278. https://doi.org/10.1029/2002JA009791

Schwinger, J. (1951). On the green's functions of quantized fields. I. *Proceedings of the National Academy of Sciences of the United States of America*, *37*(7), 452–455. https://doi.org/10.1073/pnas.37.7.452

Shklyar, D. R., & Matsumoto, H. (2011). Oblique whistler-mode waves in the inhomogeneous magnetospheric plasma: Resonant interactions with energetic charged particles. *Surveys in Geophysics*, *30*, 55–104. https://doi.org/10.1007/s10712-009-9061-7

Soto-Chavez, A. R., Bhattacharjee, A., & Ng, C. S. (2012). Chorus wave amplification: A free electron laser in the Earth's magnetosphere. *Physics of Plasmas*, *19*(1), 010701. https://doi.org/10.1063/1.3676157

Tao, X. (2014). A numerical study of chorus generation and the related variation of wave intensity using the DAWN code. *Journal of Geophysical Research: Space Physics*, *119*, 3362–3372. https://doi.org/10.1002/2014JA019820

Tao, X., Li, W., Bortnik, J., Thorne, R. M., & Angelopoulos, V. (2012). Comparison between theory and observation of the frequency sweep rates of equatorial rising tone chorus. *Geophysical Research Letters*, *39*, L08106. https://doi.org/10.1029/2012GL051413

Tao, X., Thorne, R. M., Li, W., Ni, B., Meredith, N. P., & Horne, R. B. (2011). Evolution of electron pitch-angle distributions following injection from the plasma sheet. *Journal of Geophysical Research*, *116*, A04229. https://doi.org/10.1029/2010JA016245

Tao, X., Zonca, F., & Chen, L. (2017a). Identify the nonlinear wave-particle interaction regime in rising tone chorus generation. *Geophysical Research Letters*, *44*, 3441–3446. https://doi.org/10.1002/2017GL072624

Tao, X., Zonca, F., & Chen, L. (2017b). Investigations of the electron phase space dynamics in triggered whistler wave emissions using low noise δf method. *Plasma Physics and Controlled Fusion*, *59*(9), 094001. https://doi.org/10.1088/1361-6587/aa759a

Tao, X., Zonca, F., & Chen, L. (2021). A "trap-release-amplify" (tara) model of chorus waves. *Journal of Geophysical Research: Space Physics*, *126*, e2021JA029585. https://doi.org/10.1029/2021JA029585

Tao, X., Zonca, F., Chen, L., & Wu, Y. (2020). Theoretical and numerical studies of chorus waves: A review. *Science China Earth Sciences*, *63*(1), 78–92. https://doi.org/10.1007/s11430-019-9384-6

Thorne, R. M., Li, W., Ni, B., Ma, Q., Bortnik, J., Chen, L., & Kanekal, S. G. (2013). Rapid local acceleration of relativistic radiation-belt electrons by magnetospheric chorus. *Nature*, *504*, 411–414. https://doi.org/10.1038/nature12889

Thorne, R. M., Ni, B., Tao, X., Horne, R. B., & Meredith, N. P. (2010). Scattering by chorus waves as the dominant cause of diffuse auroral precipitation. *Nature*, *467*, 943–946. https://doi.org/10.1038/nature09467

Trakhtengerts, V. Y., Demekhov, A. G., Titova, E. E., Kozelov, B. V., Santolik, O., Gurnett, D., & Parrot, M. (2004). Interpretation of cluster data on chorus emissions using the backward wave oscillator model. *Physics of Plasmas*, *11*(4), 1345–1351. https://doi.org/10.1063/1.1667495

Tsurutani, B. T., Chen, R., Gao, X., Lu, Q., Pickett, J. S., Lakhina, G. S., et al. (2020). Lower-band "monochromatic" chorus riser subelement/wave packet observations. *Journal of Geophysical Research: Space Physics*, *125*, e2020JA028090. https://doi.org/10.1029/2020JA028090

Tsurutani, B. T., & Smith, E. J. (1974). Postmidnight chorus: A substorm phenomenon. *Journal of Geophysical Research*, *79*(1), 118–127.

van Hove, L. (1954). Quantum-mechanical perturbations giving rise to a statistical transport equation. *Physica*, *21*(1), 517–540. https://doi.org/10.1016/S0031-8914(54)92646-4

Vomvoridis, J. L., Crystal, T. L., & Denavit, J. (1982). Theory and computer simulations of magnetospheric very low frequency emissions. *Journal of Geophysical Research*, *87*(A3), 1473–1489. https://doi.org/10.1029/JA087iA03p01473

Weinstock, J. (1969). Formulation of a statistical theory of strong plasma turbulence. *The Physics of Fluids*, *12*(5), 1045–1058. https://doi.org/10.1063/1.2163666

Wu, Y., Tao, X., Zonca, F., Chen, L., & Wang, S. (2020). Controlling the chirping of chorus waves via magnetic field inhomogeneity. *Geophysical Research Letters*, *47*, e2020GL087791. https://doi.org/10.1029/2020GL087791

Zhang, X.-J., Mourenas, D., Artemyev, A. V., Angelopoulos, V., Kurth, W. S., Kletzing, C. A., & Hospodarsky, G. B. (2020). Rapid frequency variations within intense chorus wave packets. *Geophysical Research Letters*, *47*, e2020GL088853. https://doi.org/10.1029/2020GL088853

Zonca, F., Chen, L., Briguglio, S., Fogaccia, G., Milovanov, A. V., Qiu, Z., & Wang, X. (2015). Energetic particles and multi-scale dynamics in fusion plasmas. *Plasma Physics and Controlled Fusion*, *57*(1), 014024. https://doi.org/10.1088/0741-3335/57/1/014024

Zonca, F., Chen, L., Briguglio, S., Fogaccia, G., Vlad, G., & Wang, X. (2015). Nonlinear dynamics of phase space zonal structures and energetic particle physics in fusion plasmas. *New Journal of Physics*, *17*(1), 031052. https://doi.org/10.1088/1367-2630/17/1/013052

Zonca, F., Tao, X., & Chen, L. (2017). Nonlinear wave-particle dynamics in chorus excitation In *44th EPS Conference on Plasma Physics* (Vol. 41F). Northern Ireland: Belfast.